DYNAMICAL PHENOMENA IN NEMATIC LIQUID CRYSTALS INDUCED BY LIGHT

D. O. Krimer,[1] G. Demeter,[2] and L. Kramer[1]

[1]*Physikalisches Institut der Universitaet Bayreuth, D-95440 Bayreuth, Germany*

[2]*Research Institute for Particle and Nuclear Physics of the Hungarian Academy of Sciences, Konkoly-Thege Miklos ut 29-33, H-1121 Budapest, Hungary*

Abstract A wide range of interesting dynamical phenomena have been observed in nematic liquid crystals in the past decades, that are induced by strong laser radiation. We review the latest theoretical advances in describing and understanding these complex phenomena.

Keywords: Nematic liquid crystals, Dynamical phenomena, Optically induced instabilities

Introduction

The optics of liquid crystals has been a widely investigated subject for decades, whose importance stems in the enormous range of technological applications where liquid crystals are utilized for their optical properties. The most important advantage of liquid crystals is that these optical properties can be changed and controlled quickly and easily. The basic physical origin of these phenomena is the subject of a number of review papers [1, 2] and monographs [3, 4].

A very interesting group of phenomena are those associated with the so-called light-induced director reorientation in nematic liquid crystals (or nematics for short). Liquid crystals consist of elongated molecules (rod shaped, or disc shaped), which have anisotropic polarizability. In a nematic liquid crystal phase, where the molecular orientation is ordered, the propagation of light waves is then governed by an anisotropic dielectric tensor. The optical axis of the nematic is aligned along the local direction of the molecular axis, which is called the director. On the other hand, the anisotropic polarizability also means that an orienting torque is exerted on the molecules by any electrical field - including the electric field of the light. Thus an intense light, whose electric field is strong enough to reorient the molecules (i.e. turn the director), alters the optical properties of the medium it propagates through. This leads to a large

variety of nonlinear optical responses of the liquid crystal medium. Some of these phenomena are rather spectacular (such as the ring pattern due to light self-phase modulation) and are sometimes collectively referred to as the Giant Optical Nonlinearity of liquid crystals [1, 2].

Among these phenomena, there are a number of situations where a constant illumination of the liquid crystal leads to persistent oscillation of the molecules, and sometimes even to chaotic behaviour. There has been considerable effort recently to observe, describe and understand these phenomena. A lot of experiments have been performed and theoretical models have been proposed. In some cases, there is sufficient agreement between theory and experiment, in other cases not. In all cases it is clear that the dynamical behaviour excited by light in nematics is very rich - numerous bifurcations, transitions and regimes have been predicted and observed. In this paper we review recent theoretical developments in modeling, simulating and understanding the physical origins of these phenomena. We put special emphasis on explorations in the "nonlinear domain", where considerable progress has been made during the past few years. Numerous instabilities and bifurcations were found and they helped interpret experimental observations a great deal. By no means is the task accomplished however - there are a number of experimental situations which have been considered theoretically only very superficially, or not at all. Understanding these complex phenomena is, as yet, far from complete.

1. Simple setups - complicated phenomena

The basic experimental setup that can be used to generate the complex nonlinear behaviour in nematics is deceptively simple. A thin cell is made from two parallel glass plates enclosing the nematic layer, whose thickness is the order of $L = 10 - 100\mu m$. The glass plates are coated with some chemical surfactant to achieve a fixed orientation of the nematic director at the interface. The cell is irradiated with a continuous laser beam, and the reorientation of the molecules induced by the light is monitored by measuring the changes in intensity and polarization of the outcoming light. Sometimes a separate probe beam is used whose changing polarization and intensity supplies information on director reorientation (Fig. 1). The key properties of the setup are the thickness of the nematic layer, the orientation of the director at the boundaries, the polarization, angle of incidence, and intensity of the light.

Depending on the relative orientation of the vector of polarization of light and the initial director orientation, we can distinguish two different cases. In one case, the two directions enclose some angle $0 < \beta < \pi/2$ and so an orienting torque acts, that turns director for arbitrarily small light intensity - there is no threshold intensity required (though considerable intensity may be needed for appreciable changes in the director orientation as the elasticity

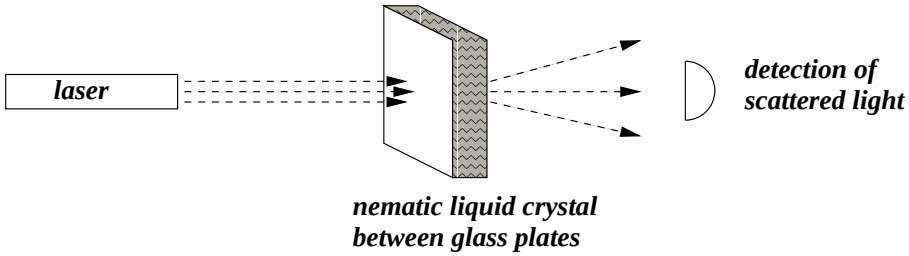

Figure 1. Typical experimental setup: a thin layer of nematic liquid crystal is sandwiched between two glass plates and irradiated with laser light. The scattered light (or the light of a probe beam) is monitored behind the cell.

of the nematic counteracts the reorientation). In the other case the director orientation is parallel or perpendicular to the polarization vector, and so the orienting torque acting on the director is zero. However, even though the configuration where the director is perpendicular to the polarization is always an equilibrium, above a certain light intensity it will be unstable. Thus above a certain threshold intensity director reorientation will take place. This is the so called Light-Induced Freedericksz Transition or Optically Induced Freedericksz Transition (OFT) [1, 3], which is analogous to the classical Freedericksz transition induced by static (or low frequency) electric or magnetic fields. This transition can already lead to time dependent behaviour in certain geometries, in other geometries the simple static reoriented state undergoes further bifurcations as the light intensity increases, and produces complex, time dependent behaviour.

2. Theoretical description

Basic equations

The starting point for the description of these complex phenomena is the set of hydrodynamic equations for the liquid crystal and Maxwell's equation for the propagation of the light. The relevant physical variables that these equations contain are the director field $\mathbf{n}(\mathbf{r},t)$, the flow of the liquid $\mathbf{v}(\mathbf{r},t)$ and the electric field of the light $\mathbf{E}_{light}(\mathbf{r},t)$. (We assume an incompressible fluid, and neglect temperature differences within the medium.) The Navier-Stokes equation for the velocity $\mathbf{v}$ can be written as [5]

$$\rho_m \left(\partial_t + \mathbf{v}\cdot\nabla\right) v_i = -\nabla_j (p\,\delta_{ij} + \pi_{ij} + T^{visc}_{ij}) \,, \tag{1}$$

where ρ_m and p are the density and the pressure of the nematic, respectively. π_{ij} is the Ericksen stress tensor defined as

$$\pi_{ij} = \frac{\partial F}{\partial(\partial_j n_k)} \cdot \partial_i n_k \quad i = x, y, z \tag{2}$$

(Summation over doubly occurring indices is assumed.) In Eq. (2) F is the free energy density which consists of the elastic part

$$F^{(elast)} = \frac{K_1}{2} (\nabla \cdot \mathbf{n})^2 + \frac{K_2}{2} (\mathbf{n} \cdot \nabla \times \mathbf{n})^2 + \frac{K_3}{2} (\mathbf{n} \times \nabla \times \mathbf{n})^2 \tag{3}$$

and the external part which in our case is

$$F^{(ext)} = -\frac{\varepsilon_a}{16\pi} \mid \mathbf{n} \cdot \mathbf{E}_{light} \mid^2 . \tag{4}$$

Here K_1, K_2, K_3 are, respectively, the splay, twist and bend elastic constants [5] and $\mathbf{E}_{light}$ is the amplitude of the optical electric field. Any other external fields which act on the director (static or low frequency electric or magnetic fields for example) can be incorporated into $F^{(ext)}$ by adding similar terms. The viscous stress tensor T_{ij}^{visc} in Eq. (1) is written in terms of the six Leslie coefficients α_i [6],

$$\begin{aligned} -T_{ij}^{visc} &= \alpha_1 n_i n_j n_k n_l A_{kl} + \alpha_2 n_j N_i + \alpha_3 n_i N_j + \\ &\quad \alpha_4 A_{ij} + \alpha_5 n_j n_k A_{ki} + \alpha_6 n_i n_k A_{kj} . \end{aligned} \tag{5}$$

The symmetric strain-rate tensor A_{ij} and the vector $\mathbf{N}$, which gives the rate of change of the director relative to the fluid, are

$$\begin{aligned} A_{ij} &= (\partial_i v_j + \partial_j v_i)/2 , \\ \mathbf{N} &= (\partial_t + \mathbf{v} \cdot \nabla)\mathbf{n} - \boldsymbol{\omega} \times \mathbf{n} . \end{aligned} \tag{6}$$

Here $\boldsymbol{\omega} = (\nabla \times \mathbf{v})/2$ is the local fluid rotation. The Leslie coefficients satisfy the Parodi relation $\alpha_2 + \alpha_3 = \alpha_6 - \alpha_5$ [7]. In addition, the assumption of incompressibility means that the density ρ_m is constant and so $\nabla \cdot \mathbf{v} = 0$. The equation for the director $\mathbf{n}$ is

$$\gamma_1(\partial_t + \mathbf{v} \cdot \nabla - \boldsymbol{\omega}\times)\mathbf{n} = -\underline{\underline{\delta}}^{\perp} (\gamma_2 \underline{\underline{A}}\mathbf{n} + \mathbf{h}) , \tag{7}$$

where $\gamma_1 = \alpha_3 - \alpha_2$ is the rotational viscosity and $\gamma_2 = \alpha_3 + \alpha_2$. $\mathbf{h}$ is the molecular field obtained from the variational derivatives of F:

$$h_i = \frac{\delta F}{\delta n_i} = \frac{\partial F}{\partial n_i} - \partial_j \left(\frac{\partial F}{\partial n_{i,j}} \right) , \quad i = x, y, z . \tag{8}$$

and the projection operator $\delta_{ij}^{\perp} = \delta_{ij} - n_i n_j$ in Eq. (7) ensures conservation of the normalization $\mathbf{n}^2 = 1$.

In addition, the electric field must be obtained from Maxwell's equations for light propagation, which, for a nonmagnetic material in the absence of any currents and charges can be written as:

$$\begin{aligned} \nabla \times \mathbf{H} &= \frac{1}{c}\underline{\underline{\varepsilon}}\,\frac{\partial \mathbf{E}}{\partial t}, \qquad \nabla \cdot (\underline{\underline{\varepsilon}}\,\mathbf{E}) = 0 \\ \nabla \times \mathbf{E} &= -\frac{1}{c}\frac{\partial \mathbf{H}}{\partial t}, \qquad \nabla \cdot \mathbf{H} = 0 \end{aligned} \tag{9}$$

with the spatially dependent dielectric tensor

$$\varepsilon_{ij} = (\varepsilon_\perp + i\gamma_\perp)\,\delta_{ij} + (\varepsilon_a + i\gamma_a)\,n_i n_j, \tag{10}$$

where $\varepsilon_a = \varepsilon_\parallel - \varepsilon_\perp$ [$\gamma_a = \gamma_\parallel - \gamma_\perp$] is the real [imaginary] part of the dielectric anisotropy. The imaginary part which describes absorption is usually negligible in pure nematics, but must be taken into account if the nematic has been doped by absorbing dyes.

The boundary conditions needed for an unambiguous solution of the PDEs are usually taken to be a fixed orientation of the director (strong anchoring) and vanishing velocity field (no-slip) at the nematic-glass interface.

The equations (1), (7) and (9) constitute the starting point for any theoretical description of dynamical phenomena induced by light in nematics. Clearly, light propagation is influenced by the spatial distribution of the director orientation through the dielectric tensor (10), and the electric field of the light influences the orientation of the director through the free energy (4) whose derivatives (8) enter the director equation (7). The fluid flow must also be added, as flow is coupled to the director, so any dynamical process that leads to director reorientation will also induce flow even in the absence of pressure gradients. This is the so-called backflow.

Some general remarks

The above equations contain three distinct timescales: the time it takes the light to traverse the cell $\tau_l = L/c$, the momentum diffusion time $\tau_{visc} = \varrho_m L^2/\gamma_1$ and the director relaxation time $\tau = \gamma_1 L^2/\pi^2 K_3$. These usually differ by many orders of magnitude, since typically $\tau_l \sim 10^{-13} s$, $\tau_{visc} \sim 10^{-6}\, s$ and $\tau \sim 1s$, so the slow variable of the system is clearly the evolution of the director which enslaves the other two modes. The electric field of the light can thus be expressed from Maxwell's equations as a function of the instantaneous value of $\mathbf{n}$, and can be considered as a self-consistency relation or a constraint. In a similar way, due to the vastly different magnitude of τ and τ_{visc}, inertial terms in the Navier-Stokes equation can be neglected and the flow of the nematic can be expected to be determined entirely by the director components and their time derivatives.

These equations are a very complex set of nonlinear partial differential equations. The main difficulty lies in the fact that even though, $\mathbf{E}_{light}$ and $\mathbf{v}$ are theoretically defined by $\mathbf{n}$ at every instant t, in general it is very hard, if not impossible to express them by $\mathbf{n}$. Most often we can only say that "$\mathbf{E}_{light}$ and $\mathbf{v}$ are a solution of this and that", where "this and that" will be a partial differential equation. Even when $\mathbf{E}_{light}$ and $\mathbf{v}$ can be expressed by $\mathbf{n}$, the expressions will be complicated integral relationships. To gain any meaningful solutions (even using computers) one must resort to further assumptions and approximations. Analytic results are available only under the most restrictive approximations and simplest cases. Numerical solutions are obtainable under much less restrictive conditions, but yield proportionally less insight into the physical origin of the phenomena. A delicate balance is needed when applying restrictive assumptions to the solutions in order to obtain solvable equations, and at the same time to keep physical phenomena within grasp. Should the assumptions be too restrictive, we will readily obtain solutions that miss important aspects of the dynamics or have no connection with real physical processes at all. A constant comparison between theoretical results and experimental observations is needed to avoid pitfalls.

There are several major simplifications that can be used to tackle these equations. First of all, fluid flow is almost always neglected altogether. Then the Navier-Stokes equation is not needed at all, $\mathbf{v}$ is no longer a variable and we only need to solve the director equation (7) which will now be

$$\gamma_1 \partial_t \mathbf{n} = -\underline{\underline{\delta}}^{\perp} \mathbf{h}. \tag{11}$$

$\mathbf{h}$ will still contain the electric fields through (4) and (8), so (11) is still coupled to (9). This approximation is sometimes justified by arguments that flow plays only a passive role (backflow) and makes only a quantitative difference. Sometimes it is argued that when reorientation is small, the effect of flow can be included in a renormalized (reduced) rotational viscosity. This however, turns out not always to be true. A renormalized viscosity is applicable strictly only in a linear approximation (even then not always) and backflow turns out to make a qualitative difference in some cases. Thus the real reason why flow is usually neglected is simply because it reduces the complexity of the equations a great deal. Explicit treatment of backflow has been attempted only in very few cases [8–10]. Even without flow, obtaining $\mathbf{E}$ from $\mathbf{n}$ remains a formidable task and usually more approximations are needed.

Another frequently employed simplification is the 1D assumption, namely that all variables depend only on one coordinate, the one transversal to the plane of the nematic layer, say the z coordinate. This means that the incident light should be an infinite plane wave (hence this approximation is often called the infinite plane wave approximation) and, by virtue of incompressibility and the boundary conditions $\mathbf{v} = (v_x(z,t), v_y(z,t), 0)$ which grants an enormous

simplification of the initial equations [9]. The application of this assumption is slightly controversial. Experimental setups rarely use laser beams whose width w_0 is so much larger than that of the cell L, that would justify it. Also, there is evidence that even if the laser beams were ideal plane waves, transverse degrees of freedom could not be neglected, for spontaneous pattern formation would occur [11, 12] (see the last section). However, current experimental evidence leads us to believe that the width of the laser beam w_0 plays a crucial role in the observed phenomena only if the cell width L is about two times larger ($w_0/L \approx 0.5$) [13]. Theoretical results derived using the 1D assumption compare remarkably well to experimental observations obtained using laser beams with $w_0/L \approx 1$. Due to this, the 1D assumption is relaxed very rarely.

In the 1D approximation the director equations (7) reduce to [9]:

$$\begin{aligned} \gamma_1 \partial_t n_x + n_z \left[(\alpha_2 - \gamma_2 n_x^2) \partial_z v_x - \gamma_2 n_x n_y \partial_z v_y \right] &= -\left[\underline{\underline{\delta}}^{\perp} \mathbf{h} \right]_x \\ \gamma_1 \partial_t n_y + n_z \left[(\alpha_2 - \gamma_2 n_y^2) \partial_z v_y - \gamma_2 n_x n_y \partial_z v_x \right] &= -\left[\underline{\underline{\delta}}^{\perp} \mathbf{h} \right]_y . \end{aligned} \quad (12)$$

Following the concept of adiabatic elimination, the velocity gradients $\partial_z v_x, \partial_z v_y$ can be expressed with the components of $\mathbf{n}$ from (1) and substituted into (12) [14, 9]. The procedure is straightforward, but expressions are complicated, so the equations obtained can be solved only numerically.

A further simplification which can be made comes from the typical boundary condition of strong anchoring which allows to expand the z dependence of the director in terms of a full set of base functions, typically trigonometric functions. Since elasticity in nematics inhibits the growth of reorientation with a force proportional to k_i^2 (here k_i is the inverse wavelength of the i-th mode), high order modes will be strongly damped and thus a truncation to a finite number of modes is possible. This way, spatial dependence with respect to z is described by a few mode functions and their amplitudes. If additionally the 1D assumption is also used (i.e. the physical quantities depend only on z), this procedure of expansion and projection of the equations onto the base functions can be used to get rid of spatial dependence altogether. The system reduces to a finite dimensional one, described by a set of complicated nonlinear ODEs for the mode amplitudes. This is favorable, as investigating the solutions of nonlinear ODEs is almost always much simpler, even if, in this case not necessarily faster. On the other hand, taking too few modes can easily result in a loss of physically important solutions. In any case, a correct choice of director description (Cartesian components, various angles, e.g. spherical) is essential. Choosing a representation that corresponds to the symmetries of the setup can simplify the equations drastically.

It is important to note, that the inhibition of high order modes due to elasticity always holds - even when it is not easy or practical to utilize. Thus sometimes a numerical solution of the equations does not use such an expan-

sion, but the results are projected onto a set of modes for analysis, as the time behaviour of mode amplitudes is often more meaningful and telling than the time behaviour of the director at any one point within the cell.

Equations for the light propagation

The most basic and unavoidable of problems when treating dynamical phenomena induced by light in nematics is the solution of Maxwell's equations for some distorted director configuration. Phenomena in the nonlinear domain are governed by an interplay between director reorientation - light torque change due to modification of light propagation, so the success or failure of a theory often depends on the suitably chosen representation and/or approximations used when dealing with this problem.

One simplification can almost always be applied: since director reorientation changes very slowly on the spatial scale of the wavelength of light, the electric field can be separated into fast phase exponentials and slow amplitudes (similarly to many problems of light propagation in anisotropic media). If additionally the 1D assumption can be applied, it is possible to write relatively simple coupled ODEs for the slow field amplitudes (the amplitudes will depend only on z - slow time dependence will result only through the time dependence of the director). One possible way to obtain equations for slow amplitudes in the 1D case is to use the so-called Berreman formalism [15]. The electric and magnetic fields of the light should be written in the form:

$$\mathbf{E}_{light}(\mathbf{r},t) = \frac{1}{2}(\mathbf{E}(z,t)e^{i(k_x x + k_y y)}e^{-i\omega t} + c.c.), \tag{13}$$

with the possible $x - y$ dependence of the fields due to oblique incidence entirely incorporated into the fast exponentials. From (9), or the wave equation that can be obtained from it, it is straightforward to derive an equation for the amplitudes $\mathbf{E}(z,t), \mathbf{H}(z,t)$. A vector of four independent amplitudes describes the light field and a set of linear, first order, ordinary differential equations governs its evolution:

$$\frac{d\bar{\Psi}}{dz} = ik_0 \mathsf{D}\bar{\Psi}, \tag{14}$$

where

$$\bar{\Psi} = \begin{pmatrix} E_x \\ H_y \\ E_y \\ -H_x \end{pmatrix} \tag{15}$$

The matrix D depends on the director components [3] and the other two field components are defined by the above four unambiguously. By calculating the

eigenvalues of D, one can separate the fast oscillations in z from the slow amplitudes. Another frequently used formalism is the separation of the electric field into an ordinary and an extraordinary wave component [3]. This separation depends on space and time through the director components, but the resulting equations are very useful (especially for the case of perpendicular incidence), as the slow amplitudes change only due to twist distortions of the nematic which is often small enough to allow a perturbative solution of the equations.

If the equations of motion (1,7 or 11) are to be integrated by computer, the equations for the slow field amplitudes can be solved numerically relatively easily at each step of the integration. Sometimes it is also possible to obtain an approximate expression for the fields as a function of the director components. This is not very easy, however, and great care must be taken. While the amplitudes of the electric field may change relatively slowly as the light traverses the cell, phase differences between various components acquire importance much faster. This means that integrals of the director components will appear in the expressions and perturbation theory has a very limited validity.

3. Obliquely incident, linearly polarized light

One of the most interesting and investigated geometries is when a linearly polarized light wave is incident at a slightly oblique angle on a cell of homeotropically aligned nematic. The direction of polarization is perpendicular to the plane of incidence in this setup - so the system is symmetric with respect to inversion over this plane [the $x - z$ plane, see Fig. 2 (a)]. Very interesting dynamical phenomena were observed in numerous experiments in this geometry. First it was noted that persistent oscillations are possible above a certain threshold intensity [16, 17]. Then various "competing" oscillatory states and

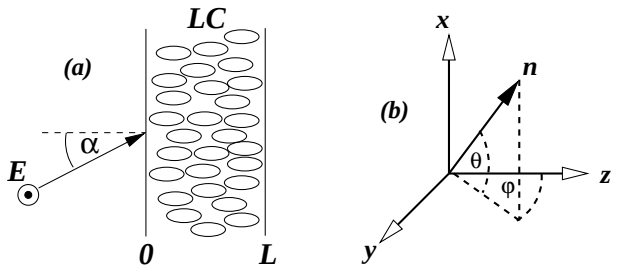

Figure 2. Basic geometry of the setup. A linearly polarized light wave is incident upon a cell of homeotropically aligned nematic at a slightly oblique angle α. The direction of polarization is perpendicular to the plane of incidence (ordinary wave). The setup is symmetric with respect to the inversion $S:\ y \to -y$.

stochastic oscillations were found [18] and it was noted that the system eventually exhibits chaotic behaviour [19]. Considerable effort went into exploring the various regimes of regular and stochastic oscillations and trying to identify the transitions between them [20, 21]. Without a detailed theory however, interpretation of experimental observations remained inadequate. Initial theoretical investigations performed the linear stability analysis of the homeotropic state [16, 22]. These treatments used the 1D approximation, neglected flow, and, employing a mode expansion, managed to derive a solvable set of linear equations for small distortions around the homeotropic state. They showed that the first instability of the homeotropic state is a pitchfork bifurcation for small angles (the usual optical Freedericksz transition), but above a certain angle of incidence α_{TB} the primary instability becomes a Hopf bifurcation. However, since the angles at which regular oscillations and stochastic behaviour were observed were smaller than this critical angle, it was obvious that one must go beyond the linear stability analysis and look for further bifurcations in the nonlinear regime.

The next step was the derivation of a "simple" model to try describe these complex phenomena [23]. The starting point was again the same as that used previously for the linear stability analysis: a plane wave approximation for the light, no flow included and the assumption that reorientation is small around the homeotropic state, i.e. we are in the weakly nonlinear regime. The director was described in terms of two angles as $\mathbf{n} = (\sin\theta, \cos\theta \sin\varphi, \cos\theta\cos\varphi)$ [see Fig. 2 b)] and using the strong anchoring at the boundary these were expanded as $\varphi(z,t) = \sum_n A_n(t) sin(n\pi z/L)$, $\theta(z,t) = \sum_n B_n(t) sin(n\pi z/L)$. The set of mode amplitudes $(A_1, .., B_1, ...)$ were truncated, the resulting expression for the director substituted into the equations of motion and projected onto these modes. The aim of this analysis was to derive a set of explicit first order ODEs for the time evolution of the mode amplitudes. Clearly, for a "minimal model" expected to be able to describe further bifurcations and possibly chaotic oscillations, one needs to keep at least three mode amplitudes, and keep nonlinear terms up to at least third order. The difficult point of this analysis was the solution of Maxwell's equations analytically, with the mode amplitudes as parameters, which was accomplished using perturbation theory exploiting the fact that the reorientation angles are expected to be small. (Note that this choice of angles is different from the one usually used, namely the spherical angles. The reason is that with spherical angles only the polar coordinate can be assumed to be small, the azimuthal one not - thus a power

expansion is not possible.) The general form of the equations obtained is:

$$\begin{aligned}
\tau\dot{A}_i &= \sum_j L^A_{ij}A_j + \sum_{j,k} P^A_{ijk}A_jB_k \\
&\quad + \sum_{\substack{j,k,l \\ k\le l}} Q^A_{ijkl}A_jB_kB_l + \sum_{j\le k\le l} R^A_{ijkl}A_jA_kA_l, \\
\tau\dot{B}_i &= \sum_j L^B_{ij}B_j + \sum_{j\le k} P^B_{ijk}A_jA_k + \sum_{\substack{j,k,l \\ k\le l}} Q^B_{ijkl}B_jA_kA_l \\
&\quad + \sum_{j\le k\le l} R^B_{ijkl}B_jB_kB_l\,. \qquad (16)
\end{aligned}$$

The inversion symmetry with respect to the $x-z$ plane implies that the equations must be invariant under the transformation $S:\{A_i,B_i\}\to\{-A_i,B_i\}$, so that only odd powers of the A_i-s can appear in the first set of equations and only even powers in the second set. In a linear approximation, only the A-s have to be taken into account, as they are the ones driven by the light directly. Thus for a minimal model the three modes: A_1, A_2, B_1 have been kept. The resulting set of ODEs has been solved numerically, and the nature of the solutions analyzed as a function of the two control parameters of the problem, the angle of incidence α and the intensity of the light normalized by the OFT threshold ρ.

The numerical solution of the equations gave exciting results. In the region where the primary instability of the homeotropic state is a stationary instability, two new stationary states are born, which are mutual images under the symmetry transformation S. These then lose stability at some critical intensity in a Hopf bifurcation, where two limit cycles are born (again, mutual images under S). They are depicted on Fig. 3 a) where they are plotted in the phase space spanned by the three amplitudes $\{A_1, A_2, B_1\}$. This is very reassuring, since it accounts for the regular oscillating regime observed in the experiments for angles smaller than α_{TB}. As the intensity is increased, the symmetric limit cycles pass closer and closer to the origin (which, above the OFT threshold is saddle) and at a certain intensity ρ_1 they become homoclinic trajectories to the origin (i.e. the homogeneous homeotropic state) [Fig. 3 b)]. Above ρ_1 the two limit cycles merge into one double-length limit cycle that is symmetric with respect to S, [Fig. 3 c)]. This bifurcation is called a homoclinic gluing, or a gluing bifurcation. A further increase in the light intensity then brings about another symmetry-breaking bifurcation, where the symmetric limit cycle gives way to two new asymmetric limit cycles, mutual images under S [Fig. 3 d)]. At a still higher intensity these too become homoclinic to the origin [Fig. 3 e)] and merge into a quadruple-length symmetric limit cycle [Fig. 3 f)]. This sequence of splitting and re-merging of limit cycles continues ad infinitum, and

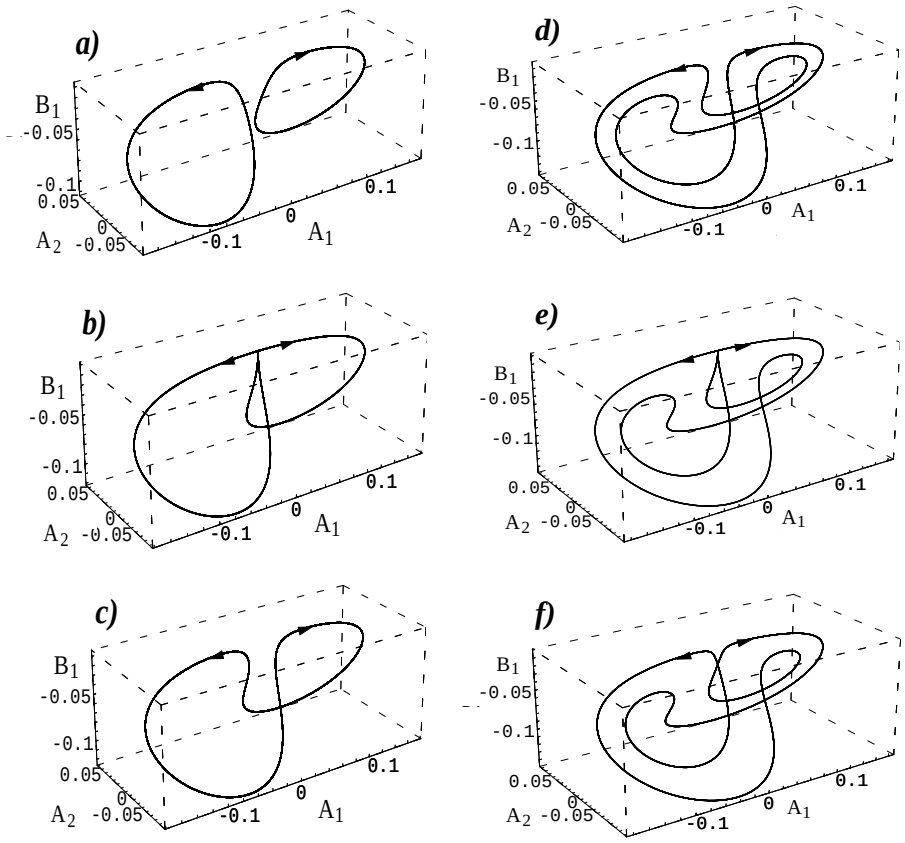

Figure 3. Limit cycles in phase space at various intensities as obtained from the simple model and $\alpha = 7^{\circ}$. a) $\rho = 1.78$ b) $\rho = 1.80875$, c) $\rho = 1.85$, d) $\rho = 1.94$, e) $\rho = 1.9474$ f) $\rho = 1.96$.

the bifurcation thresholds ρ_i converge to certain value ρ_∞. Beyond this point the motion is chaotic, the system moves along a strange attractor in phase space [Fig. 4]. The system exhibits typical signatures of low-dimensional deterministic chaos such as great sensitivity to initial conditions and a positive Lyapunov exponent. The frequency spectrum of the mode amplitudes also shows this transition to chaos by changing from a line spectrum (where all lines are integer multiples of the same fundamental frequency) to a continuous spectrum. We would like to emphasize: while this route to chaos involves the birth of double-length limit cycles at a sequence of points, it is very different from the usual period doubling scheme as the stable homoclinic limit cycle at the bifurcation has an infinite period. This quite distinct route to chaos was analyzed in

a series of papers [24, 25], but to our knowledge has never been observed in an experiment before.

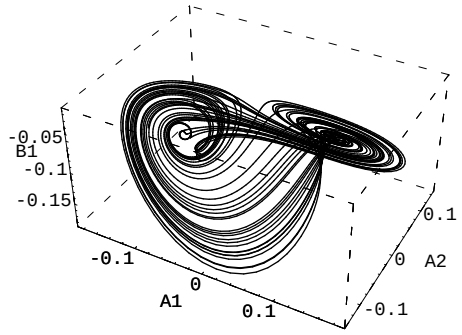

Figure 4. Strange attractor in phase space at $\alpha = 7^\circ$ and $\rho = 2.18$.

Apart from this peculiar route to chaos, there was a great variety of interesting nonlinear behaviour found in this simple model in various domains of the parameter plane spanned by the angle of incidence α and the intensity of light ρ [23]. The most important result of the model is, however that the first region of regular oscillation - stochastic oscillation - regular oscillation which was found in various experiments [19, 21] could be interpreted in terms of the system passing through the first gluing bifurcation. As the system is in the immediate vicinity of this bifurcation and orbits are close to being homoclinic trajectories to the origin, there are random transitions between orbits (or different parts of the same orbit) due to noise in the experiment. Thus two "competing" modes of oscillations exist with random transitions between them. Some distance below and above the bifurcation, the limit cycles do not approach the vicinity of the origin and there are no random jumps. Therefore the evolution of the system seems regular above and below the bifurcation, but is found to be stochastic in the immediate vicinity. This interpretation is made even more convincing by a reconstruction of the limit cycles from experimental data [26], which shows clearly that the symmetry properties of the trajectories above and below the bifurcation change precisely as expected. However, for higher intensities the agreement between the predictions of the model and the observations was not good. Experiments revealed what looked like another gluing bifurcation (whose nature was different from the one expected for the second gluing in the model) another periodic regime, then an abrupt transition to chaotic behaviour. This was found at intensities much higher than the intensities where chaos exists in the model.

Thus, while the simple model was successful in identifying the first two bifurcations above the primary one, experimental results did not confirm the existence of the full cascade of gluing bifurcations leading to chaos. To gain further insight into dynamical phenomena, a numerical study of the equations was performed [27]. This study retained the assumption that light can be described by a plane wave and it also neglected flow. The assumption that reorientation is small was relaxed. Using a finite differences algorithm the equations were first solved, and mode amplitudes characterizing the motion of the system in phase space were extracted from the solution. The result of this treatment was somewhat surprising. The first three bifurcations the system goes through (Freedericksz transition, secondary Hopf and first gluing) was the same as in the simple model. (Although there was a considerable difference in the bifurcation threshold for the gluing bifurcation.) For higher intensities however, the cascade of gluing bifurcations was not found. Furthermore, the observed dynamical scenarios were different from that observed experimentally and chaos was not found in the simulations for the parameters the experiments were performed with. This made it clear that although higher order nonlinearities that were neglected in the simple model do play a major role in the dynamics of the system, further assumptions must be discarded for a correct description of the phenomena.

Clearly, the next step in refining theoretical description of these phenomena had to be the relaxation of one of the major assumptions and either include flow in the equations, or discard the plane wave approximation and consider narrow beams. Since other experimental works that investigated dynamical phenomena induced by narrow laser beams indicated that the beam width becomes an important parameter only when it is about two times smaller than the cell width [13], the choice was to include flow and treat light as a plane wave. Thus another numerical study of the system was performed, along similar lines as the previous one. This time the full nematodynamical equations including flow were solved [10]. The results of this calculation were much more satisfying. The first three bifurcations (primary, secondary Hopf and first gluing) occurred in the same way as in the simple model and the first simulation. There were only quantitative differences of the bifurcation thresholds (Fig. 5 shows the lines of the most important bifurcations on the $\rho - \alpha$ plane. The lines of the primary Hopf bifurcation and the first gluing bifurcation are shown as calculated from both simulations, so that the difference between the bifurcation thresholds caused by the inclusion of flow can be seen.) As the intensity is increased, the bifurcation scenario is qualitatively different for the calculation with flow. There is a second gluing bifurcation as observed in the experiments, but its nature is different from that suggested by the model. It is actually the inverse of the first one - the symmetric limit cycle breaks up into two small asymmetric limit cycles like those depicted on Fig. 3 a). After

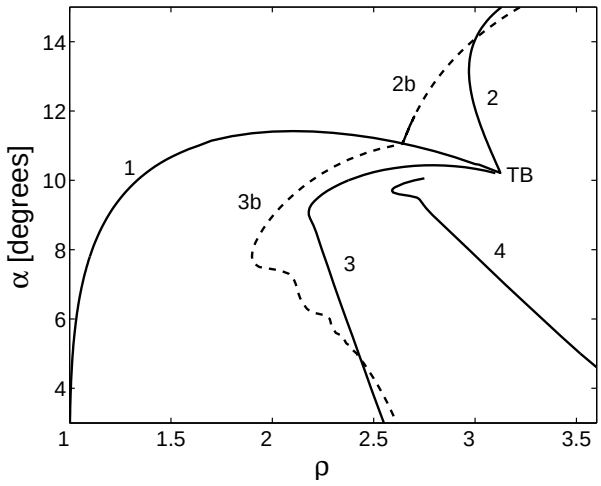

Figure 5. Bifurcation diagram on the plane of the two control parameters ρ and α. The solid lines 1 and 2 mark the primary instability, where the homogeneous homeotropic orientation becomes unstable. At 1 the bifurcation is a stationary (pitchfork) bifurcation, at 2 a Hopf one. The two lines connect in the Takens-Bogdanov (TB) point. The solid lines 3 and 4 mark the first gluing bifurcation and the second gluing bifurcation respectively. The dashed lines 2b and 3b mark the lines of the primary Hopf bifurcation and the first gluing bifurcation when calculated without the inclusion of flow in the equations.

this second gluing, a strange attractor appears abruptly as the intensity is increased. This sequence now agrees with the dynamical scenarios observed in the experiments, so it appears that the calculation that includes flow is capable of interpreting experimental observations at all intensities. It also proves that flow plays a major part in the dynamics when the light intensity is high enough, so it is imperative to take flow into account if observations are to be interpreted correctly. This supports the assumption that finite beam size effects can be neglected even though these experiments too were performed with $w_0/L \approx 1$.

Another exciting result of the calculation with flow was, that the route to chaos via a cascade of gluing bifurcations was actually located in the parameter plane, close to the Takens-Bogdanov point. Since bifurcation lines are nearly parallel to the ρ axis in this region, they can be traversed by keeping the intensity fixed and decreasing the angle of incidence. The scenario can be found in a region which was not explored by experiments, so the existence of this very peculiar route remains to be confirmed by a further experiment.

4. Perpendicularly incident, circularly polarized light

Another intriguing geometry to which much attention was attracted during the last two decades is when a circularly polarized beam is incident perpendicularly on a layer of nematic that has initially homeotropic alignment. The light is polarized in the plane of the layer (the x-y plane) and propagates along the positive **z** axis (see Fig. 6). In this case the optical Freedericksz transition is observed to be weakly hysteretic, and above threshold the molecules undergo a collective rotation [28] (that corresponds to a uniform precession of the director). This effect is well understood in the frame of a purely classical (hydrodynamic) approach [28]. The fact that the director rotates above the transition rather than settling to some stationary or oscillating state can be explained by symmetry. Contrary to the geometry discussed in the previous section, the present one possesses isotropic symmetry in the plane of the layer. Thus the only states allowed are rotating ones (the peculiar case of stationary distortion can be regarded as a rotation whose frequency becomes zero). Another explanation in terms of ordinary (*o*) and extraordinary (*e*) waves is also possible. When the director has homeotropic alignment, the phase speeds of *e* and *o* waves are the same, so the phase difference $\alpha(z)$ between *e* and *o* waves remains $\pi/2$. Thus light polarization is unchanged and remains circular when it propagates through the nematic layer. When the director reorients, $\alpha(z)$ changes because the phase speed of the e-wave travelling across the layer depends on z. Thus the polarization becomes elliptic inside the layer. The light-torque acting on the director tries to turn it towards the major axis of polarization, leading to precession.

The subcritical nature of the Freedericksz transition can be explained as follows. When the director settles to the precession state, light becomes elliptically polarized inside the nematic. On the other hand, it is known that the Freedericksz transition for elliptically polarized light depends on ellipticity,

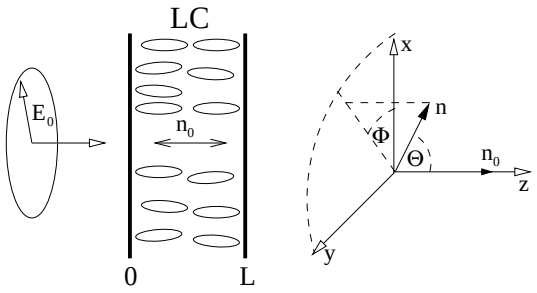

Figure 6. Geometry of the setup: circularly polarized light incident perpendicularly on a nematic layer with the director $\mathbf{n_0} \parallel \mathbf{z}$ (homeotropic state). The components of the director $\mathbf{n}$ are described in terms of the angles Θ, Φ ($\Theta = 0$ in the homeotropic state).

and occurs at some intensity between the Freedericksz threshold for linearly polarized light and the one for circularly polarized light (see the next section). (The threshold for OFT for circularly polarized light is two times higher than that for a linearly polarized one.) Thus, once reorientation takes place, the elliptically polarized light that develops inside the nematic can sustain the distortion even if the intensity is decreased slightly below the initial threshold.

The precession of the molecules can also be interpreted in a quantum picture as spin angular momentum transfer from the light to the medium and is called self-induced stimulated light scattering [29]. Since collective molecular rotation dissipates energy, the light beam has to transmit part of its energy to the medium. As the pure nematic LC is a transparent medium (no absorption) this energy loss leads to a red shift of a part of the light beam [29]. The mechanism can be described as follows: each scattered photon has its helicity reversed and thus transfers an angular momentum of $2\hbar$ (that is perpendicular to the layer) to the medium. Moreover its energy is lowered by an amount $\hbar\Delta\omega$. Thus p photons per unit time produce a constant torque $\tau_z = 2\hbar p$, acting on the medium, which induces a collective molecular precession. This torque is balanced by the viscous torque. The angular velocity of the uniform precession Ω is related to the red shift $\Delta\omega$ by the simple formula $\Delta\omega = 2\Omega$. This formula can be derived from energy conservation using that i) p photons loose per unit time the amount of energy $\hbar\Delta\omega p$; ii) the work made by the torque τ_z on the director is $\tau_z\Omega = 2\hbar p\Omega = \hbar\Delta\omega p$. The fact that in the final relation $\hbar$ disappears, shows that one can obtain this formula through a classical approach [30].

In general the angular momentum of the light beam consists of two parts: a spin part associated with polarization [31] and an orbital part associated with spatial distribution [32]. However, if the spatial distribution in the plane of the layer is supposed to be homogeneous i. e. when one deals with a plane wave approximation, then the orbital part is zero. In this context it may be interesting to note that laser light with a Laguerre-Gaussian amplitude distribution can be shown to have a well-defined orbital angular momentum [33].

The theoretical description of the OFT in this geometry was reported in [34] where the importance of twist deformations of the director was pointed out and the hysteretic nature of the OFT was explained. In [30] a theoretical and experimental investigation of the dynamical behavior of the system for the region of higher intensities was reported. The authors of [30] observed a further discontinuous transition with large hysteresis from a precession regime with small reorientation amplitude occurring above the OFT to one with large reorientation. The frequency of the large amplitude precession was found to be much smaller than the one just above the OFT and to exhibit rapid variations with the incident intensity reaching zero at roughly periodic intervals. In this work the authors presented an approximate model that can describe qualitatively both

regimes of uniform director precession and also presented clear experimental evidence of the frequency reduction in the second regime.

Again, one of the simplifications used in this model was the infinite plane wave approximation. Under this assumption, all relevant functions depend solely on the spatial coordinate z and the time t. Obviously, the representation adapted to this geometry is the one given in usual spherical angles $\Theta(z,t)$ and $\Phi(z,t)$ such that $\mathbf{n} = (\sin\Theta\cos\Phi, \sin\Theta\sin\Phi, \cos\Theta)$ [see Fig. 6]. The twist angle is written then as $\Phi = \Phi_0(t) + \Phi_d(z,t)$, where $\Phi_0(t)$ does not depend on z and describes a rigid rotation of the director around the z axis (no distortion) while $\Phi_d(z,t)$ contains twist distortion. Such a decomposition is not unique in the sense that any constant can be added to Φ_0 and then subtracted from Φ_d. The key point, however, is that Φ_0 depends on time only and can be unbounded while Φ_d is required to remain bounded. (Note that nonzero Φ_d means that the instantaneous director profile is out of plane.) To construct a simple model, some further simplifying hypotheses are needed [30], namely i) the backflow is neglected; ii) the splay-bend distortion are small, i.e., $\Theta^2(z,t) \ll 1$; iii) a sine trial function for $\Theta(z,t)$ is used; iv) the twist distortions are small, i.e., $|\partial_z \Phi_d| \ll 1/L$; v) the slow-envelope approximation for Maxwell's equations can be used. Retaining terms up to third order in Θ and keeping the lowest order terms in $\partial_z\Phi_d$, the following expressions for the frequency of the uniform director precession $2\pi f_0 = d\Phi_0(t)/dt$ and the twist gradient $\partial_z\Phi_d$ have been obtained:

$$f_0 = \frac{\rho\,(1-\cos\Delta)}{2\pi\Delta}\,,\ \partial_z\Phi_d = \frac{\pi\rho}{2\Delta}\,\frac{(1-\cos\Delta)v(z) - 1 + \cos[\Delta v(z)]}{\sin^2 z}\,, \quad (17)$$

where time and length are normalized as $t \to t/\tau$ and $z \to \pi z/L$, respectively. Here ρ is the normalized intensity such that $\rho = 1$ corresponds to the threshold for OFT and $v(z) = (z - \sin z\cos z)/\pi$. Δ is the phase delay induced by the whole layer and is a global measure of the amplitude of reorientation. It has a direct experimental interpretation, since the quantity $\Delta/2\pi$ represents roughly the number of self diffraction rings in the far field [35] and, under the approximation used, is proportional (with a large prefactor) to the square of the amplitude of the polar angle $\Theta_1^2(t)$. Finally, an analytic solution for $\Delta(\rho)$ has been found [30] which is given by a rather cumbersome formula. As is seen from Eq. (17) f_0 indeed becomes smaller and exhibits rapid variation with increasing Δ (i.e. with increase of the reorientation).

Even though the approximate model gave a satisfactory description of the observed phenomena, the nature of the transition from one regime to the other was not understood in this framework. Some years later, a qualitative mechanism based on non-uniform spin angular momentum deposition from the light to the nematic was introduced to explain the origin of such a transition [36]. A particular interest to this problem arose again more recently, when an addi-

tional continuous secondary instability between the OFT and the abrupt transition to the largely reoriented state was observed [37]. Although a preliminary description of the bifurcation scenario was reported in [38] the global scenario was still obscure. It became clear that a numerical study is needed to gain better insight to the problem [39, 40]. The original problem consisting of two PDEs for Θ and Φ was simplified by means of expansions of Θ and Φ_d with respect to z in systems of orthogonal functions which satisfy the boundary conditions: $\Theta = \sum_{n=1}^{\infty} \Theta_n(t) \, \sin nz$, $\Phi_d = \sum_{n=1}^{\infty} \Phi_n(t) \, \sin(n+1)z/\sin z$. After substituting these expansions into the director equations with further projecting the equation for Θ onto the modes Θ_n and one for Φ onto Φ_n (Galerkin method), a set of coupled nonlinear ODEs for the modes Θ_n and Φ_n has been derived. To solve this set which contains the field amplitudes, the two ODEs for the field amplitudes have to be integrated dynamically at each step of numerical integration for time t [40]. The infinite set of ODEs was reduced to a finite one by truncating the mode expansion for Θ and Φ_d. It is worth noting that for a state of uniform director precession (UP) [$f_0 = const$] the set of ODEs reduces to one of nonlinear algebraic equations for Φ_n and Θ_n which become constant in time. The results of this numerical study which explains the entire scenario is discussed in what follows.

In Fig. 7, the phase delay $\Delta/2\pi$ is plotted versus the normalized intensity ρ. The solid lines represent stable uniform precession (UP) states, while the dashed lines correspond to precession states that are unstable. The region in gray corresponds to a nonuniform precession (NUP) where nutation ($d\Delta/dt \neq 0$) is coupled to precession. In this regime, the lower and the upper lines that limit the region correspond to the minimum and maximum values taken by Δ during its oscillation.

The OFT occurs at $\rho = 1$ via a subcritical Hopf-type bifurcation where the system settles to a uniform precession state with a small reorientation amplitude ($\Delta \sim \pi$ so that $\Theta^2 \ll 1$) labeled UP1. Decreasing the intensity from the UP1 regime, the system switches back to the unperturbed state at $\rho = \rho_1^* \simeq 0.88$ where a saddle-node bifurcation occurs. The trajectory in the (n_x, n_y) plane is a circle whereas in a coordinate system that rotates with frequency f_0 around the z axis it is a fixed point. The time Fourier spectra of the director $\mathbf{n}$ have one fundamental frequency f_0, whereas Θ_n, Φ_n and Δ do not depend on time.

It is worth noting here that from the weakly nonlinear analysis it follows [40] that the nature of the OFT is governed by the sign of the coefficient $C = K_1/K_3 - (9/4)\,(\varepsilon_a/\varepsilon_{||})$. $C < 0$ corresponds to a subcritical OFT while $C > 0$ corresponds to a supercritical OFT. Incidentally, this criterion is identical to the one derived in the case of OFT under linearly polarized light [41]. In present example, $C = 0.154$ and the OFT is actually supercritical. However, the solution branch turns over and becomes subcritical (and unstable) already

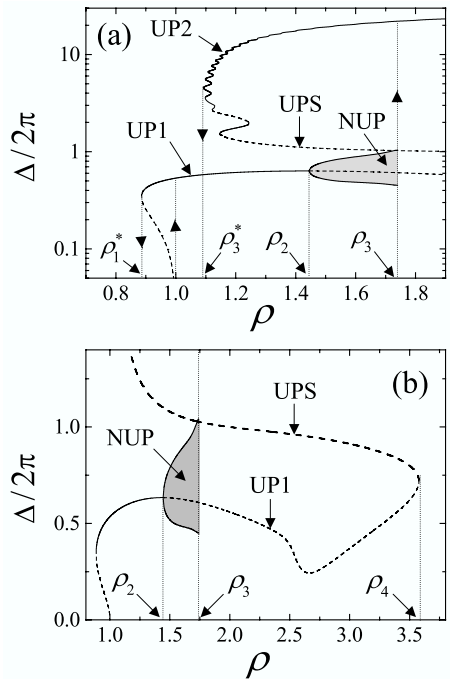

Figure 7. (a) $\Delta/2\pi$ on a log scale versus ρ for $\rho < 2$ and $\Delta < 50\pi$. (b) $\Delta/2\pi$ on a linear scale versus ρ for $\rho < 4$ and $\Delta < 3\pi$. Solid (dashed) curves correspond to stable (unstable) solutions.

at $\rho = 1 + \delta\rho$ where $\delta\rho \simeq 10^{-6}$. This explains why the OFT appears to be subcritical on the scale used in Fig. 7. In fact, although $\delta\rho$ increases when the cell thickness is decreased, even at $L = 10$ μm, the subcritical region is still too small to detect ($\delta\rho \simeq 10^{-4}$).

With further increase of the intensity, the UP1 state looses stability via a supercritical Hopf bifurcation at $\rho = \rho_2$ where the director starts to nutate (NUP regime). For the NUP state all modes Θ_n and Φ_n with $n \geq 1$ are time dependent and their Fourier spectrum contains frequencies mf_1, where m is an integer. The spectra of the phase delay Δ, director $\mathbf{n}$ have contributions at frequencies given by the simple formulas: $\tilde{\Delta} = \{mf_1\}, \tilde{\mathbf{n}} = \{f_0, mf_1 \pm f_0\}$. In some narrow region around $\rho_3 \approx 1.75$ the period $T = 1/f_1$ of the NUP increases progressively with increasing light intensity, and indeed appears to diverge logarithmically at ρ_3, as is shown in Fig. 8. Thus as ρ approaches ρ_3, the NUP limit cycle collides with the unstable UPS branch which is a saddle. In fact we deal here with a homoclinic bifurcation of the simplest type where a limit cycle collides with a saddle point having only one unstable direction

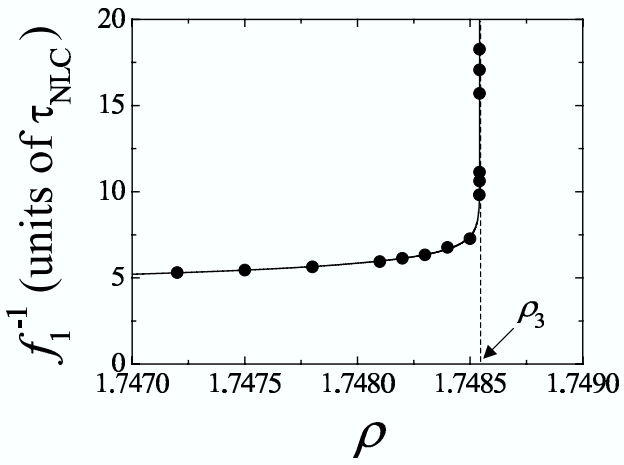

Figure 8. Characterization of the homoclinic bifurcation $f_1^{-1}(\rho) = \mathcal{O}[\ln(\rho_3 - \rho)]$ near ρ_3 ($\rho_3 = 1.748542389055$). The solid line is the best fi t to the theoretically calculated values (•).

[42] (all the eigenvalues have negative real parts except one, which is real and positive).

At $\rho = \rho_3$ the system jumps to a new state of uniform precession of the director (UP2) with large reorientation ($\Theta \simeq 74^o$) and slow precession rate. As displayed in Fig. 7, starting from the stable UP2 branch above ρ_3 and lowering the excitation intensity, one finds a large and rather complicated hysteretic cycle, which eventually flips back to the UP1 solution at $\rho_3^* = 1.09$. This part of the UP2 branch consists of alternatively stable and unstable regions exhibiting a series of saddle-node bifurcations. Eventually this branch connects with the UPS one which makes a loop and connects with the UP1 branch.

As a result of the appearance of the new frequency f_1 at $\rho = \rho_2$, the director motion becomes quasi-periodic characterized by the two frequencies f_0 and f_1. This is illustrated in Fig. 9(a) where the trajectory of the director in the (n_x, n_y) plane is plotted for $\rho = 1.55$ at some z inside the layer. This trajectory is not closed in the laboratory frame indicating quasi-periodicity of the director. In fact, the two independent motions, namely the precession (f_0) and the nutation (f_1) can be isolated by transforming to a frame that rotates with frequency f_0. In the rotating frame, the director performs a simple periodic motion with frequency f_1 as is seen in Fig. 9(b) with the arrow indicating the sense of rotation for the case where the incident light is left circularly polarized. (The sense of rotation is always opposite to that of the underlying precession [43].) As is seen from Fig. 9(c,d) starting from initial conditions near the unstable UP1 solution or the UPS one, the director eventually settles on the NUP solution, which is represented by a simple limit cycle.

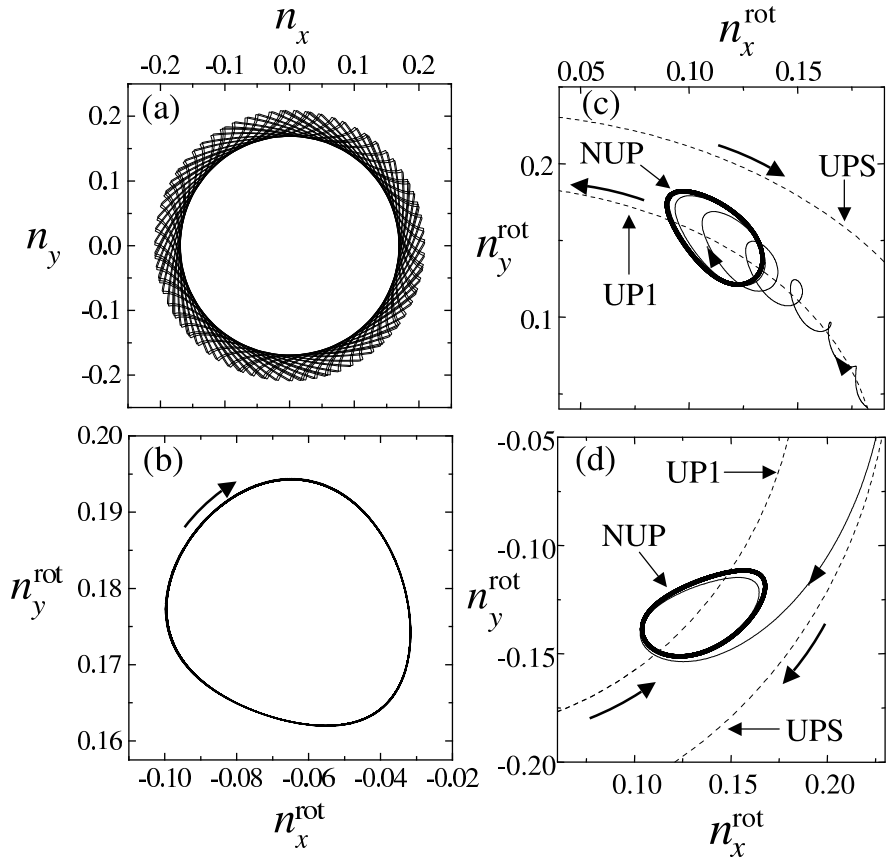

Figure 9. (a),(b): director trajectory at $\rho = 1.55$. (a) Quasiperiodic behavior in the laboratory frame (n_x, n_y). (b) Periodic limit cycle in the rotating frame $(n_x^{\rm rot}, n_y^{\rm rot})$. The arrow indicates the sense of rotation when the incident light is left circularly polarized.
(c),(d): director trajectory at $\rho = 1.55$ in the $f_0(\rho, {\rm NUP})$-rotating frame showing the instability of the UP1 and UPS solutions in the NUP regime. (c) Initial condition near the UP1 solution. (d) Initial condition near the UPS solution. The arrows indicate the sense of rotation of the corresponding trajectory when the incident light is left circularly polarized.

In fact, the unstable UPS branch represents the saddle point (or separatrix) that separates the regions of attraction of the NUP state (or, below ρ_2, the UP1 state) from that of the largely-reoriented UP2 state. At this point it might also be interesting to note that the UP1 state represents a stable node at $\rho \sim \rho_1$ (the relevant stability exponents are real and negative). Then, between ρ_1 and ρ_2 it changes to a focus (the stability exponents become complex). At ρ_2 the real part of the complex pair of stability exponents passes through zero and then becomes positive.

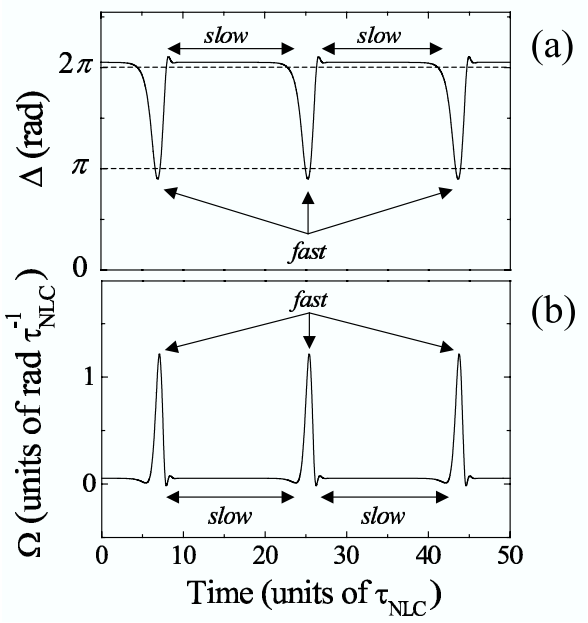

Figure 10. Calculated dynamics just below $\rho = \rho_3$. (a) Phase shift $\Delta(t)$. (b) Instantaneous angular velocity $\Omega(t) = d\Phi_0/dt$.

As ρ approaches the homoclinic bifurcation point, the trajectory of the director approaches the unstable UPS orbit for longer and longer intervals. The dynamics near ρ_3 possesses two time scales, a slow and a fast one, as expected from the homoclinic nature of the transition. Figure 10 emphasizes this point where the phase shift $\Delta(t)$ and the instantaneous angular velocity $\Omega(t) = d\Phi_0/dt$ are plotted versus time.

The bifurcation scenario discussed above was actually observed in the experiment. Although a good qualitative agreement between theory and experiment was found [40] there are quantitative discrepancies. In the experiment the measured onset of the nutation-precession motion turns out to be about 20% lower than predicted by theory. Moreover the slope of the precession frequency versus intensity predicted by theory turned out to be different from that observed in the experiment. One of the two possible reasons could be the use of finite beam size in the experiment (that is typically of the order of the thickness of the layer) whereas in theory the plane wave approximation was assumed. Actually, the ratio δ between diameter of the beam and the width of the layer is another bifurcation parameter (in the plane wave approximation $\delta \to \infty$) and was shown to play crucial role on the orientational dynamics [13]. There and in [44] the importance of the so called walk-off effect was pointed out which consists of spatial separation of Pointing vectors of the ordinary and

extraordinary waves. (Ideally this effect disappears when the propagation takes place along the principal axis, i.e. the director $\mathbf{n}$.) The problem in this case has to include lateral degrees of freedom and becomes much more complicated. An appropriate theoretical description is still missing. The other reason could be neglection of the fluid velocity in the LC. In [9] the influence of backflow on the director dynamics was examined. After adiabatic elimination of the flow field, a linear stability analysis around the basic state has been performed in order to assess the "linearized viscosity reduction factor". As expected the threshold for the OFT is unchanged whereas the growth rate $\sigma = (\rho - 1)/(\tau\xi)$ acquires an additional factor $\xi < 1$ ($\xi = 1$ corresponds to neglection of backflow). Thus, within the linear approximation, backflow results in a renormalization of the rotational viscosity γ_1 (in fact a reduction). The same expression for the reduction factor ξ was found in [8] where a one-mode approximation for the director components and smallness of the twist distortion were used.

As was demonstrated in [9] backflow does not lead to qualitative changes in the dynamical scenario, but does lead to substantial quantitative changes in the secondary bifurcation threshold. It turns out that the regime of nonuniform precession shifts to higher light intensities by about 20% and exists in a larger interval. In Fig. 11, $\Delta/2\pi$ is plotted versus the normalized intensity ρ. The phase delay Δ for the UP regimes is only slightly different from the case without backflow. However, the regime of nonuniform director precession shifts to higher intensities. As is seen from Fig. 11 the thresholds for the

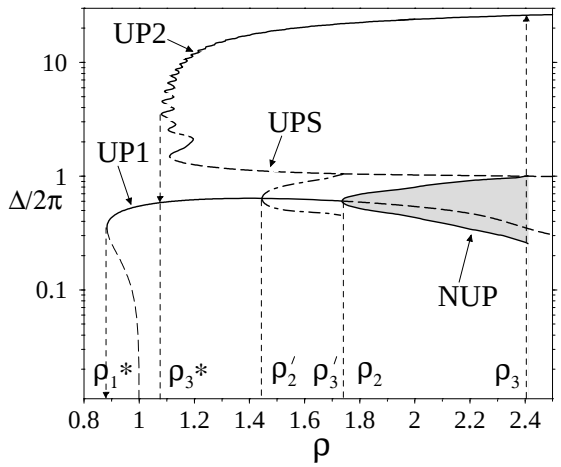

Figure 11. $\Delta/2\pi$ versus ρ in semi-logarithmic scale. Solid (dashed) curves correspond to stable (unstable) UP solutions. Gray region: nonuniform precession states of the director. Dash-dotted lines in the (ρ_2', ρ_3') interval: nonuniform precession states of the director when backfbw is neglected. The fact that $\rho_3' \simeq \rho_2$ is accidental.

NUP and for the UP2 regimes turns out to be $\rho_2 = 1.75$ and $\rho_3 = 2.4$ instead of $\rho_2' = 1.45$ and $\rho_3' = 1.75$ when the backflow is neglected [39, 40]. In [9] was also shown that the precession frequency f_0 for UP1 states actually increases when the backflow is included (as expected because γ_1 effectively decreases). An unanticipated spatial oscillation of the backflow in the UP2 regime were also found which results from spatial oscillations of the director twist $\partial_z\Phi$. They are a consequence of oscillations in the torque resulting from interference phenomena between ordinary and extraordinary light. The backflow behaves very differently for the three types of the director motion and, thus, can act as a sensitive diagnostic to distinguish them.

Thus, the inclusion of backflow made the situation even worse because the experimental values of the thresholds ρ_2, ρ_3 are even smaller than that given by the theory without backflow [39, 40]. One is forced to conclude that the discrepancy between the theoretical predictions and the experiment is strongly affected by the fact that in the experiments the beam size was not large compared to the layer thickness. By using a large aspect-ratio geometry one is now in a position to test the theoretical framework [9] quantitatively. This can be done by use of a dye-doped nematic because the values of OFT in this case can be two orders of magnitude smaller than for a pure nematic (see [45, 46] and references therein). The fact that the threshold intensity is low allows the spot size of the light to be much larger than the thickness of the layer, thus the plane wave approximation assumed in the theory might be better achieved in the experiment.

5. Perpendicularly incident, elliptically polarized light

A natural generalization of the previous geometry is an elliptically polarized (EP) plane wave incident perpendicularly on a layer of nematic that has initially homeotropic alignment (see Fig. 6 in the previous chapter). The ellipticity $-\pi/4 \leq \chi \leq \pi/4$ is related to the ratio between the minor and the major axis of the polarization ellipse. The case $\chi = 0$ [$\chi = \pm\pi/4$] corresponds to a linearly [circularly] polarized light. The sign of χ determines the handedness of the polarization, thus it is sufficient to choose $\chi > 0$ only. The main difference with the CP light discussed in the previous section is the broken rotational invariance around the z-axis.

As was shown in [47] the director is unperturbed (U) until the intensity reaches a critical value that depends on χ: $I_F^{\rm EP} = I_F^{\rm CP}/(1 + \cos 2\chi)$, where $I_F^{\rm CP}$ is the intensity for OFT of CP light. Thus we have two control parameters, the ellipticity χ and the incident intensity I. In what follows the normalized intensity $\rho = I/I_F^{\rm CP}$ is used.

For $\chi < \pi/4$ the OFT is a pitchfork bifurcation and the reoriented state is a stationary distorted state (D) state. In [48], the oscillating states (O)

were experimentally observed. The numerical analysis [48] of the basic equations indeed predicts the existence of such a state. It should be noted that reflection symmetry is spontaneously broken by the first bifurcation, so in the D and O states one has two symmetry degenerate solutions related by $\{n_x \to -n_x, n_y \to -n_y\}$. In [49] a model was derived using the assumption of small director distortion, i.e. both the polar angle and the twist were assumed to be small ($\Theta^2 \ll 1$ and $\Phi_d \ll 1$). The director and the field equations were expanded then with respect to these angles and only some significant nonlinear terms were kept. Then a mode expansion for Θ and Φ was used (the same as for CP light, see previous section) and only the first mode Θ_1 for the polar angle was retained. Within this approximation the phase delay $\Delta \sim \Theta_1^2$. The equations for the Stokes vector (which determine the field amplitudes) were solved iteratively using Φ_d as a small parameter (actually the first iteration was taken). This allowed elimination of the field amplitudes from the director equations, which was finally reduced to a set of two ODEs for the phase delay Δ and the zeroth mode Φ_0 (which represents a rigid rotation). The twist modes $\Phi_{n\geq 1}$ were then assumed to follow adiabatically their steady state values and were shown to decrease rapidly with n, so only a few of them were kept. This relatively simple model was capable of predicting not only O states but also some other states occurring at higher intensities. It was demonstrated that with the increasing of ρ the transition from D to O state takes place via Hopf bifurcation, while the transition from oscillation to rotation was shown to be the gluing of two symmetrical limit cycles (for a certain region of $\chi < \pi/4$). The hysteresis between rotations and oscillations at large ellipticity χ was also predicted. It should be noted that the experimental findings [49] are qualitatively reproduced by this model.

It was shown in the previous chapter that CP light induces quasiperiodic director rotation (QPR) if the incident intensity exceeds the one for OFT by about 40% (no backflow). This is already in a higher region of intensities than that considered in [49]. So the question was what happens if one mismatches slightly from the CP case at higher intensities? It became clear [50] that a full numerical analysis is needed to capture the QPR for the elliptic case because i) the small distortion approximation failed to describe QPR for CP case; ii) higher order nonlinearities in twist terms [$\propto (\partial_z \Phi_d)^2$] are important. In [50] the QPR was found both theoretically and experimentally. Apart from this regime, other regimes of rotating, oscillating or stationary states with large director distortion and the transitions between them were predicted theoretically [50]. In what follows we present a brief overview of the bifurcation scenario following [50], which is in our opinion complete for large and moderate values of ellipticity.

Figure 12 taken from [50] presents the different regimes that exist in the (χ, ρ) plane for $0.33 \leq \chi \leq \pi/4 \simeq 0.785$. Above the OFT threshold, several

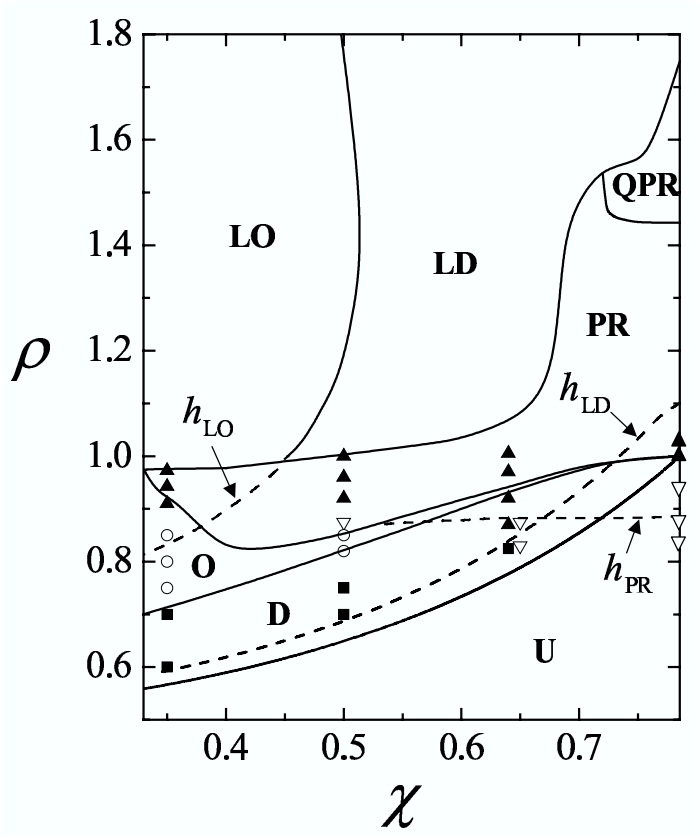

Figure 12. Phase diagram of the dynamical regimes in the parameter plane (χ, ρ). U: Undistorted state; D: stationary Distorted states; O: periodic Oscillating states; PR: Periodic Rotating states; QPR: Quasi-Periodic Rotating states; LD and LO: Large reorientation associated respectively with stationary Distorted and Oscillating states. The dashed lines $h_{\rm PR}$, $h_{\rm LD}$ and $h_{\rm LO}$ correspond to the hysteretic region of the PR, LD and LO states, respectively. The points are experimental data extracted from [49] for D (■), O (○), PR (▲) and hysteretic PR (▽).

regimes can exist depending on the values of χ and ρ: stationary distorted (D), oscillating (O), periodic rotating (PR), quasi-periodic rotating (QPR) and largely reoriented states ($\Theta \sim 1$), which may be stationary distorted (LD), oscillating (LO) or rotating (LR) states (LR states are not shown on Fig. 12 since they only arise in a narrow region $\Delta\chi \sim 10^{-2}$ near $\chi = \pi/4$). Keeping the ellipticity fixed and increasing the intensity, these regimes appear as a well-defined sequence of transitions as is summarized in Table I. The trajectories of the director in various regimes are shown in Fig. 13.

For $0.33 < \chi < 0.53$, the OFT is a pitchfork bifurcation and the reoriented state is a D state [see the filled circles in Fig. 13(a)]. This state loses its stability through a supercritical Hopf bifurcation to an O state [curve 1 in

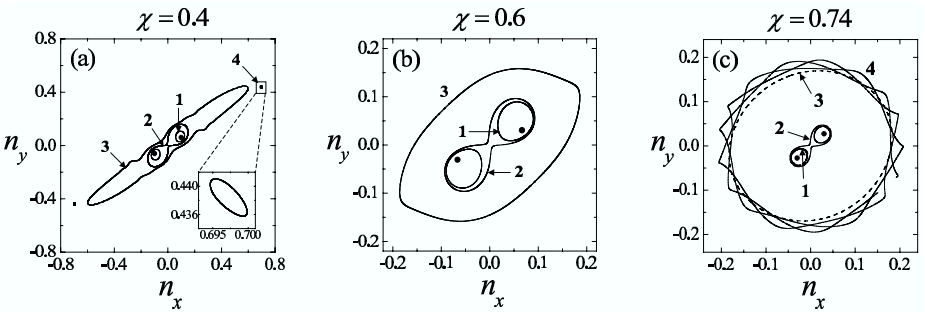

Figure 13. Calculated director trajectories in the (n_x, n_y) plane. (a) $\chi = 0.4$: stationary distorted state (D) at $\rho = 0.72$ (•); periodic oscillating state (O) at $\rho = 0.76$ (curve 1); periodic rotating state (PR) just above the gluing bifurcation at $\rho = 0.83$ (curve 2) and slightly below the transition to the largely reoriented oscillating state (LO) at $\rho = 0.97$ (curve 3); largely reoriented oscillating state at $\rho = 0.98$ (curve 4, see inset). (b) $\chi = 0.6$: stationary distorted state (D) at $\rho = 0.8$ (•); periodic oscillating state (O) at $\rho = 0.91$ (curve 1); periodic rotating state PR_1 slightly above the gluing bifurcation at $\rho = 0.917$ (curve 2); periodic rotating state PR_2 at $\rho = 0.95$ (curve 3). (c) $\chi = 0.74$: stationary distorted state (D) at $\rho = 0.99$ (•); periodic oscillating state (O) at $\rho = 0.9925$ (curve 1); periodic rotating state PR_1 slightly above the gluing bifurcation at $\rho = 0.9932$ (curve 2); periodic rotating state PR_2 slightly above the saddle-node bifurcation at $\rho = 0.9936$ (curve 3, dashed line); quasi-periodic rotating state at $\rho = 1.5$ (curve 4).

Fig. 13(a)] characterized by a single frequency f_0 (Table II). As was mentioned above the reflection symmetry is spontaneously broken by the primary bifurcation, so in the D and O states one has two symmetry degenerate solutions. As ρ increases, these two limit cycles merge in a gluing bifurcation at the origin and restore the reflection symmetry. This leads to the appearance of a single double-length limit cycle that corresponds to the trajectory in the PR state [curve 2 in Fig. 13(a)]. A further increase of the intensity eventually leads to a discontinuous transition to a largely reoriented oscillating ($\chi < 0.45$) or stationary distorted ($\chi > 0.45$) state. In both cases this transition is associated with a small relative jump of the director amplitude and corresponds to a homoclinic bifurcation. In fact, stable LO states exist until the intensity is decreased to a critical value represented by the hysteretic line h_{LO} in Fig. 12, below which the LO state becomes stationary distorted. This LD state finally vanishes when the intensity is decreased below the hysteretic line h_{LD}.

For $0.53 < \chi < 0.72$, one has the sequence U $\rightarrow$ D $\rightarrow$ O $\rightarrow$ PR as before [see Fig. 13(b)], however there is an additional bifurcation between PR states. In fact, the limit cycle amplitude of the PR regime, now labeled PR_1 [curve 2 in Fig. 13(b)], abruptly increases. This results in another periodic rotating regime labeled PR_2 with higher reorientation amplitude [curve 3 in Fig. 13(b)]. This is a hysteric transition connected to a double saddle-node structure with the (unstable) saddle separating the PR_1 and PR_2 branches, as already found

within the approximate model [49]. In that case, the system switches back to the O or D state at the line labeled $h_{\rm PR}$ in Fig. 12. In contrast, no hysteresis is observed when ρ is decreased starting from the $\rm PR_1$ regime since the O $\rightarrow \rm PR_1$ transition is continuous. The $\rm PR_1 \rightarrow PR_2$ transition is not shown in Fig. 12 because it is very near to the gluing bifurcation. At $\chi = 0.53$ the two saddle nodes coalesce. Finally, for high intensity the system switches abruptly from the $\rm PR_2$ to the LD regime. The reorientation discontinuity associated with this transition is small for $\chi < 0.66$ and quite large for $\chi > 0.66$. This due to the fact that, for $\chi < 0.66$, part of the limit cycle, associated with the PR state just below the transition, extends to large reorientations in the (n_x, n_y) plane. Consequently, it is already close to the largely reoriented states nearby [see e.g. curve 3 and 4 in Fig. 13(a)]. The transition to large reorientation is found to be a homoclinic bifurcation and when the intensity is decreased, stable LD states exist until the line $h_{\rm LD}$ is reached.

For $0.72 < \chi < \pi/4$ the sequence U $\rightarrow$ D $\rightarrow$ O $\rightarrow \rm PR_1 \rightarrow PR_2$ is observed as before [see Fig. 13(c)]. However, for higher values of ρ a QPR regime is born through a secondary supercritical Hopf bifurcation, which introduces a new frequency f_1 into the system and transforms the dynamics into a quasi-periodic behavior [curve 4 in Fig. 13(c)]. As the intensity increases the QPR state undergoes a homoclinic transition to a largely reoriented LD or LR regime, which are respectively represented by a stationary distorted or slowly rotating (close to $\chi = \pi/4$) state. This bifurcation is associated with a large discontinuity of the reorientation amplitude.

The signature of the anisotropy of incident light is visible in the director trajectories in the (n_x, n_y) plane. The PR trajectories are obviously non circularly symmetric for $\chi = 0.4$ and $\chi = 0.6$ [see Figs. 13(a,b)] whereas $\rm PR_2$ and QPR regimes are almost circularly symmetric when the polarization is almost CP [see Fig. 13(c)]. The spectral content of the variables $n_{x,y}$, Δ and $I_{x,y}$ for O, PR and QPR is listed in Table II.

Finally, one should mention the particular situation when the PR regime vanishes at $\chi = 0.33$ (see Fig. 12). There, a direct transition from the O to the LO regime occurs as the intensity is increased. The corresponding picture is this: as the intensity is increased, the limit cycle associated with the O regime collides with an unstable fixed point thus preempting the gluing at the origin. This dynamical sequence suppresses the appearance of the PR regime.

Starting from the PR or QPR regime and increasing the intensity, an instability eventually occurs at $\rho = \rho_L$ (which depends on χ, see Fig. 12) and the director settles to a largely reoriented oscillating (LO), stationary distorted (LD) or rotating (LR) state (the latter one exists in a narrow region $\Delta\chi \sim 10^{-2}$ around $\chi = \pi/4$). From Fig. 12 we see that the final state above ρ_L is a LO state if $\chi < 0.45$ and a LD state if $\chi > 0.45$. It was found that the transition from the PR or QPR regime to the largely reoriented states is related to

Table 1. Calculated sequence of bifurcations as a function of the ellipticity χ of the incident light.

Ellipticity	Sequence of transitions	Bifurcation nature
$0.33 < \chi < 0.53$	Unperturbed → Distorted	Pitchfork
	Distorted → Periodic oscillation	Supercritical Hopf
	Periodic oscillation → Periodic rotation	Gluing
	Periodic rotation → Periodic oscillation or distorted	Homoclinic [a]
$0.53 < \chi < 0.72$	Unperturbed → Distorted	Pitchfork
	Distorted → Periodic oscillation	Supercritical Hopf
	Periodic oscillation → Periodic rotation-1	Gluing
	Periodic rotation-1 → Periodic rotation-2	Saddle-node
	Periodic rotation-2 → Distorted	Homoclinic [b]
$0.72 < \chi < \pi/4$	Unperturbed → Distorted	Pitchfork
	Distorted → Periodic oscillation	Supercritical Hopf
	Periodic oscillation → Periodic rotation-1	Gluing
	Periodic rotation-1 → Periodic rotation-2	Saddle-node
	Periodic rotation-2 → Quasi-periodic rotation	Supercritical Hopf
	Quasi-periodic rotation → Distorted or periodic rotation	Homoclinic [c]
$\chi = \pi/4$	Unperturbed → Periodic rotation	Subcritical Hopf
	Periodic rotation → Quasi-periodic rotation	Supercritical Hopf
	Quasi-periodic rotation → Periodic rotation	Homoclinic [c]

[a] small jump of the director amplitude
[b] small [large] jump of the director amplitude for $\chi < 0.66$ [$\chi > 0.66$]
[c] large jump of the director amplitude

Table 2. Spectral content of the director components $n_{x,y}$, the output intensity components $I_{x,y}$ and the phase delay Δ for the different dynamical regimes for an elliptically polarized excitation.

Regime	$n_{x,y}$	$I_{x,y}$	Δ
Periodic oscillation (O)	nf_0	nf_0	nf_0
Periodic rotation (PR)	$(2n-1)f_0$	$2nf_0$	$2nf_0$
Quasi-periodic rotation (QPR)	$nf_1 \pm (2m+1)f_0$	$nf_1 \pm 2mf_0$	$nf_1 \pm 2mf_0$

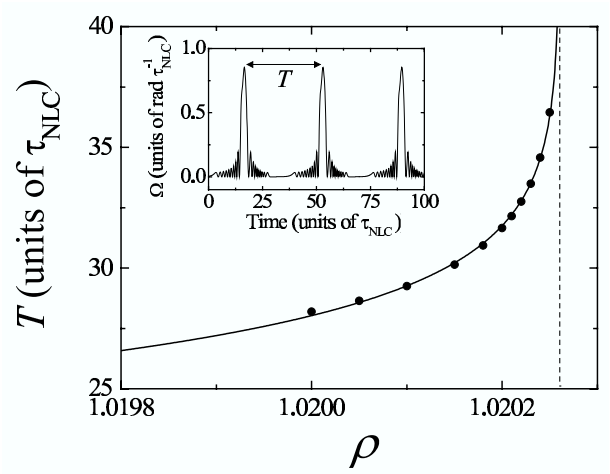

Figure 14. Characterization of the homoclinic bifurcation near ρ_L for $\chi = 0.57$, $T(\rho) = \mathcal{O}[\ln(\rho_L - \rho)]$, where T is the period of the instantaneous angular velocity $\Omega(\tau) = d\Phi_0/d\tau$. The solid line is the best fit to the theoretically calculated values (•). Inset: time evolution of $\Omega(\tau)$ at $\rho = 1.02025$. A perfect agreement with the calculated values (filled circles) is obtained with the parameterizations $a + b\ln(\rho_L - \rho)$ for $a \simeq 8.232$ and $b \simeq -2.406$ (solid line).

an increase of the period of the corresponding limit cycle. More precisely, this period appears to diverge logarithmically at $\rho = \rho_L$. This behavior is illustrated in Fig. 14 for $\chi = 0.57$. In this figure, the period of the instantaneous angular velocity $\Omega(\tau) = d\Phi_0/d\tau$ is plotted as a function ρ. The origin of this critical slowing down near the bifurcation point is illustrated in Fig. 15 where the director trajectory in the (n_x, n_y) plane is shown. Slightly below ρ_L ($\rho = 1.02025$, black solid line on the left) the trajectory approaches a saddle fixed point (open circle) during increasingly long times; this corresponds to the "plateau" behavior when $\Omega \sim 0$ in the inset of Fig. 14. On the other hand, slightly above ρ_L ($\rho = 1.02026$, gray line in Fig. 15), the director eventually settles to a stable focus (filled circle) that corresponds to a LD state. (The stable LD state in the present example [just above ρ_L for $\chi = 0.57$] is represented by a stable focus in that for lower values of χ the director settles to a LO state above ρ_L.) In fact we deal at $\rho = \rho_L$ with a homoclinic bifurcation of the simplest type where a limit cycle collides with a saddle point having only one unstable direction (all the eigenvalues have negative real part except one, which is real and positive) [42].

As was discussed in the previous section a LR state appears at high intensities for the circular case ($\chi = \pi/4$). This slow dynamics is quite fragile and disappears for perturbation of the ellipticity as small as $\Delta\chi \sim 10^{-2}$, giving rise to a LD regime instead. The mechanism for the disappearance of the LR regime is the following. In the CP limit, the precession frequency associated

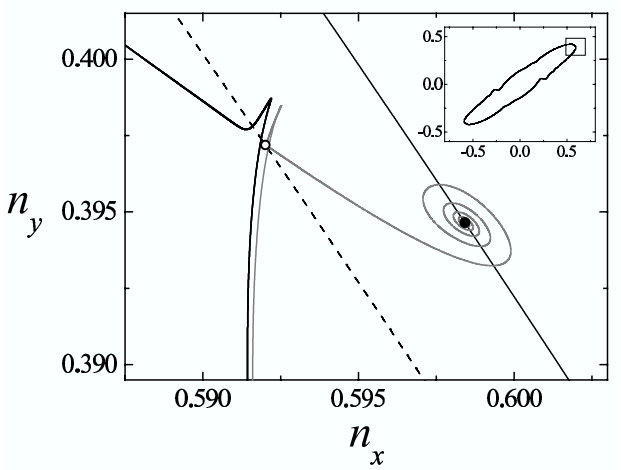

Figure 15. Director trajectory in the (n_x, n_y) plane near the homoclinic bifurcation point ρ_L at $\chi = 0.57$. Inset: homoclinic PR trajectory slightly below ρ_L ($\rho = 1.02025$). Main graph: magnifi cation of the region delimited by the box in the inset. The black solid line on the left is part of the PR trajectory at $\rho = 1.02025$ and the gray line is the transient trajectory converging to a stable fi xed point just above ρ_L ($\rho = 1.02026$). The dashed line (solid line on the right) represents the location of the unstable (stable) fi xed points in a small range of ρ centered around ρ_L. The open and fi lled circles represent respectively the unstable and the stable fi xed point at $\rho = 1.02025$ and $\rho = 1.02026$.

with the LR state exhibits almost periodic modulation as a function of the intensity with zero minimum values. As soon as the ellipticity is reduced, the points of zero frequency are transformed into finite regions which continue to increase as χ is further decreased. Eventually, these regions join leading to the LR $\rightarrow$ LD transition.

In the region of largely reoriented states, the LO regime appears for $\chi < 0.51$ [see Fig. 12]. This state is characterized in the (n_x, n_y) plane by a limit cycle with a small radius [see curve 4 in Fig. 13(a)]. It was concluded [50] that the LD states [which were stable at $\rho = \rho_L$] lose their stability at some higher value of ρ in the range $0.45 < \chi < 0.51$, leading to a LO state. In fact, the transition LD $\rightarrow$ LO takes place via a Hopf bifurcation. Moreover, these unstable LD states eventually recover their stability at higher intensities leading to the inverse transition LO $\rightarrow$ LD.

The observation of the QPR regime for ellipticities close to circular polarization gave results which agree qualitatively with the above theoretical findings [50]. To gain quantitative agreement one again should refine the theory by i) inclusion of flow; ii) taking into account the effect of finite beam size. We think, however, that neither the former, nor the latter effect would lead to substantial differences (provided the beam is not several times narrower than the cell width).

6. Finite beam-size effects and transversal pattern formation

As mentioned in the introductory sections, using the 1D assumption to solve the relevant equations of motion is a simplification that is relaxed very rarely. Although a number of works dealt with the OFT in nematics using Gaussian beam profiles [51, 52], these works dealt exclusively with the primary instability and with the properties of the stationary reoriented state above the transition in various geometries. Dynamical phenomena were not considered in any theoretical works, even though there are experiments proving that, decreasing the width of the beam yields very interesting dynamical behaviour and even chaos. One example is [13], where a circularly polarized light, incident perpendicularly on a cell of nematic was observed to induce various dynamical regimes. The ratio of the beam width to the cell width $\delta = w_0/L$ was treated as a control parameter alongside the intensity ρ, and the various bifurcation scenarios were compared as δ and ρ were changed. It was found that for $\delta \approx 0.3 - 0.4$ novel dynamical regimes and even chaotic oscillations could be observed. It was argued that a spatial mismatch between the ordinary and extraordinary waves that develops within the cell during propagation may have something to do with these phenomena. Another study [53] investigated the dynamics induced by a strongly astigmatic beam of circularly polarized light, again with normal incidence. The light of an astigmatic beam carries not just the usual spin angular momentum of circularly polarized photons, but also orbital angular momentum. It was shown in this study that as the astigmatism of the beam is increased above a certain level, (i.e. if the orbital component of the angular momentum reaches a certain ratio to the spin angular momentum component), chaotic rotation of the molecules can be observed. Both of these experiments emphasize that the laser beam shape can be an important control parameter, whose change gives rise to complex dynamics. A proper theory, however, that can account for the physical reasons, or the nature of the transitions is missing altogether.

Another possibility to consider is, that even if the light is incident on the cell as a plane wave, pattern formation may occur in the plane of the layer spontaneously. In other words, the spatially homogeneous state may loose stability to a finite wavelength perturbation, and a dependence of the physical quantities on the transverse coordinates may develop. There are several arguments to suggest that such instabilities are to be expected. On one hand, it is known [54, 55] that periodic patterns can develop in the magnetic or electric field induced Freedericksz transition in nematics, if the anisotropy of the elastic constants reaches a certain value (i.e. if three elastic constants are sufficiently different). It is also known [56], that any, almost homoclinic limit cycle is generically unstable with respect to spatiotemporal perturbations. This instability

is either a phase instability or a finite wavelength period doubling instability. This means that we can certainly expect very complicated behaviour (probably spatio-temporal chaos) to develop in the vicinity of the homoclinic bifurcations that were found in the 1D calculations in various geometries. Solving the relevant PDEs in 2 or 3 dimensions to search for transversal pattern formation phenomena would be prohibitively difficult. However, investigating the stability of various spatially homogeneous states with respect to finite wavelength perturbations is much easier and has been performed in several cases.

In [11], the simplified models of director dynamics in two geometries were examined. One was the director dynamics induced by obliquely incident, linearly polarized light. The simple model of this geometry [23] (see section 3.) was generalized to include a slow $x - y$ dependence of the amplitudes A_1, A_2, B_1. Performing a linear stability analysis of the basic state with this extended model it was found that the undistorted homeotropic state always loses stability in a spatially homogeneous bifurcation, i.e. $\vec{k}_c = 0$. (In the course of any linear stability analysis one considers spatially periodic perturbations, and the wave vector $\vec{k}$ of the mode that destabilizes the stationary state is called the critical wave vector $\vec{k}_c$ - if this is zero, the instability is said to be homogeneous.) This is true for both the stationary OFT (curve 1 on Figure 4) and the oscillatory OFT (curve 2 on Figure 4). For the case of the oscillatory OFT the relevant complex Ginzburg-Landau equation was derived which describes the behaviour of the system in the weakly nonlinear regime. The linear dispersion parameter in this equation turns out to be zero, while the nonlinear dispersion parameter is in such a range that one expects stable plane wave solutions, spirals and - in 1D - stable hole solutions [57]. The stability of the stationary distorted state above the OFT was also investigated. It was found that the secondary Hopf bifurcation which destabilizes it is homogeneous only if the Frank elastic constants are all equal ($K_1 = K_2 = K_3$), but is not homogeneous otherwise. In fact $\vec{k}_c \neq 0$ for any degree of anisotropy of the elastic constants (here reflection symmetry is broken by the primary transition, so $\vec{k}_c \neq 0$ is actually the generic case). This is contrary to the magnetic field induced transition, where there is a lower threshold to the ratio K_1/K_2 [54] or K_3/K_1 [55] below which $\vec{k}_c = 0$ and no stripes appear. Since the instability is nonstationary, a finite $\vec{k}_c$ means the appearance of travelling waves. The magnitude of $\vec{k}_c$ grows with the anisotropy of the elastic constants and its direction (the direction of wave propagation) is roughly parallel to the in-plane component of the director $\vec{n}_\perp$.

Another simple model investigated in [11] is a model of the director dynamics induced by circularly polarized light using three variables. The stability of the basic state and the uniformly precessing state above the OFT was investigated, and it was found that both of these states remain stable against any

finite k perturbation too. The phase diffusion equation for the precessing state, that describes the spatial evolution of phase disturbances [58] was also derived. The general form of this equation is $\partial_t \psi = a\nabla^2\psi + b(\nabla\psi)^2$. In our case, the spatially dependent phase perturbation is $\psi = B_0 - \Omega t$ and the real constants appearing in the equation turn out to be: $a = (K_1 + K_2)/K_3, b = 0$. This means that we have plane wave solutions ($B_0 \sim qx + py$), but without group velocity. These are the only attractors and presumably all solutions decay to such states apart from topological point defects. Vortex-like topological defects, whose core however is not described by this equation, should also exist.

The linear stability analysis of the stationary distorted state above the OFT induced by obliquely incident, linearly polarized light was repeated in [12], this time without the numerous approximations used in earlier works, using numerical methods. In addition, dye-doped nematics were considered, for which the threshold for the OFT is much lower and thus permits the experimental realization of a light beam that is much wider than the cell width. For this case, however, absorption also has to be taken into account, which means that the OFT does not happen at $\rho = 1$ for perpendicular incidence (see Fig. 16). Taking all this into account, the exact reorientation profiles for the director were calculated numerically first, and its stability was investigated with respect to spatially periodic perturbations (proportional to $exp[i(qx + py)]$). Then the

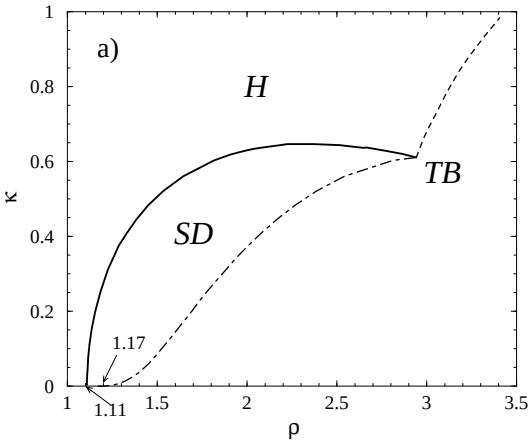

Figure 16. Bifurcation diagram of a dye-doped nematic excited by obliquely incident, linearly polarized light as a function of the intensity ρ and the dimensionless phase parameter κ, which is proportional to the $sin^2(\alpha)$. H marks the domain where the homeotropic orientation is stable. The line of OFT consists of two parts, for small angles it is a stationary bifurcation (solid line) and for higher angles a Hopf bifurcation (dashed line). The domain of stationary distortion is marked SD. The dash-dotted line marks the secondary Hopf bifurcation which gives rise to travelling waves in the plane of the layer.

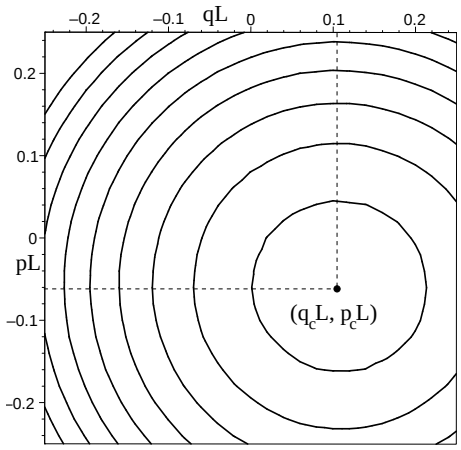

Figure 17. Contour plot of the neutral surface as a function of the dimensionless wave vector components pL and qL calculated for $\alpha = 11^\circ$. The minimum of the surface yields the critical wave vector components $q_cL = 0.11$ and $p_cL = -0.06$.

neutral surface $\rho(q, p)$ was calculated (defined by the vanishing real part for the linear growth rate for the perturbation $Re[\sigma(q, p)] = 0$ - see Fig. 17). The minimum of the neutral surface defines the components of the critical wave vector q_c, p_c, which destabilize the stationary distorted state as the intensity is increased. The intensity value $\rho(q_c, p_c)$ is the critical intensity at which the transition occurs. Since we have a nonzero wave number, and also a nonzero frequency, travelling waves are expected to appear above the transition. This analysis also confirmed, that the critical wave vector grows as the ratio of the elastic constants deviates from one, and is zero if all elastic constants are equal.

An interesting situation also came to light in the limit of normal incidence. This case was impossible to analyze in the framework of the approximate model, as the modes become large quickly and violate the initial assumptions. It turned out that for $\alpha = 0$ (which is a peculiar case since the external symmetry breaking in the x direction vanishes), another stationary instability precedes the secondary Hopf bifurcation, that spontaneously breaks the reflection symmetry with respect to x. It is shown by point A in Fig. 18. It is also seen from this figure, that the secondary pitchfork bifurcation is destroyed in the case of oblique incidence, which can be interpreted as an imperfect bifurcation with respect to the angle α [43].

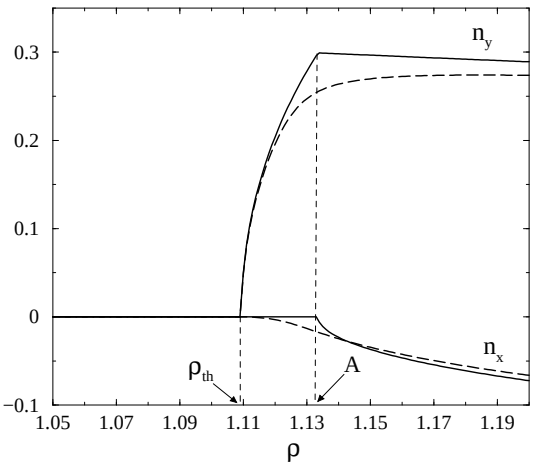

Figure 18. Profiles of the director components n_x, n_y versus ρ at some z inside the layer (not at the middle). Solid and dashed lines correspond to $\alpha = 0^\circ$ and $\alpha = 0.5^\circ$ respectively. ρ_{th} is the threshold intensity of the OFT. Point A is a pitchfork bifurcation to a stationary state with broken x-reflection symmetry ($\alpha = 0\ ^\circ$).

Conclusion and Outlook

As shown in the preceding sections, the behaviour of nematics excited by light can be extremely complex. Theoretical models reveal relatively simple reasons behind the dynamics only in a few cases. More often, experiments and elaborate computer studies show that a number of factors govern the complex behaviour together: director distortion induced by light, light propagation change due to reorientation, flow of the fluid and the effects of finite beam size all become factors to reckon with at some point or another.

There has also been a number of works devoted to some generalization of the simple system that was the subject of the present paper. One of these is the attempt to control the chaotic oscillations induced by an obliquely incident laser light with the use of additional laser beams [59]. Another one is the investigation of the response of nematics driven by circular polarized light with a periodically modulated intensity near a Hopf bifurcation. Calculations showed that the $f_1/f = 2/1$ Arnold tongue (f [f_1] is the frequency of modulation [nutation]) has a large width and there is a rather large region in the plane of amplitude - modulation frequency, where the director exhibits chaotic behaviour followed by a cascade of periodic doubling bifurcations [60]. A third example is the case of a long-pitch cholesteric liquid crystal. There the dynamics can be viewed as the result of the competition between the intrinsic unidimensional helical pattern (related with the chiral dopant) and the extrinsic one

(related with the light). It was found [61] for the case of circular polarization, that the dynamics is more complex than that for a pure nematic and depends strongly on the amount of the chiral dopant.

The study of these complex systems is important because they exhibit a large variety of nonlinear phenomena. While these are all known from the theory of nonlinear systems, many of these were investigated experimentally only in a few cases, or sometimes not at all. Therefore this relatively simple experimental system may be an important tool to realize and analyze various complex scenarios that appear in nature, and may still have many surprises in store.

Acknowledgments

Financial support by the Deutsche Forschungsgemeinschaft under contracts Kr 690/16 and 436UNG113/151/1 is gratefully acknowledged.

References

[1] N. V. Tabiryan, A. V. Sukhov and B. Ya. Zel'dovich: Mol. Cryst. Liq. Cryst. **136**, 1-140 (1985).

[2] F. Simoni and O. Francescangeli, J. Phys.: Condens. Matter **11** R439 (1999).

[3] F. Simoni, *Nonlinear optical properties of liquid crystals and polymer dispersed liquid crystals* World Scientifi c, Singapore 1997.

[4] I. C. Khoo, *Liquid Crystals: Physical Properties and Nonlinear Optical Phenomena* Wiley Interscience, New York 1994; I. C. Khoo and S. T. Wu, *Optics and Nonlinear Optics of Liquid Crystals* World Scientifi c Singapore 1993.

[5] P. G. de Gennes and J. Prost, *The physics of liquid crystals* (Clarendon press, Oxford, 1993).

[6] F. M. Leslie, Quart. J. Mech. Appl. Math. **19**, 357 (1966).

[7] O. Parodi, J. Phys. (Paris) **31**, 581 (1970).

[8] L. Marrucci, G. Abbate, S. Ferraiuolo, P. Maddalena, and E. Santamato, Mol. Cryst. Liq. Cryst. **237**, 39 (1993).

[9] D. O. Krimer, G. Demeter, and L. Kramer, Phys. Rev E **71**, 051711 (2005).

[10] G. Demeter, D. O. Krimer and L. Kramer, Phys. Rev. submitted for publication.

[11] G. Demeter and L. Kramer, Mol. Cryst. Liq. Cryst. **366**, 2659 (2001).

[12] D. O. Krimer, G. Demeter and L. Kramer, Phys. Rev. E **66**, 031707 (2002).

[13] E. Brasselet, B. Doyon, T.V. Galstian and L. J. Dube, Phys. Rev. E **69**, 021701 (2004).

[14] B. L. Winkler, H. Richter, I. Rehberg, W. Zimmermann, L. Kramer and A. Buka, Phys. Rev. A **43**, 1940 (1991).

[15] D. W. Berreman, J. Opt. Soc. Am. **62**, 502 (1972).

[16] B. Ya. Zel'dovich, S. K. Merzlikin, N. F. Pilipetskii, A. V. Sukhov and N. V. Tabiryan, JETP Lett **37**, 677 (1983).

[17] A. S. Zolot'ko, V. F. Kitaeva, N. Kroo, N. N. Sobolev, A. P. Sukhorukov, V. A. Troshkin and L. Csillag, Sov. Phys. JETP **60**, 488 (1984); V. F. Kitaeva, N. Kroo, N. N. Sobolev, A. P. Sukhorukov, V. Yu. Fedorovich, and L. Csillag, Sov. Phys. JETP **62**, 520 (1985).

[18] A. S. Zolotko, V. F. Kitaeva, N. N. Sobolev, V. Yu. Fedorovich, A. P. Sukhorukov, N. Kroo and L. Csillag, Liq. Cryst. **15**, 787 (1993).

[19] G. Cipparrone, V. Carbone, C. Versace, C. Umeton, R. Bartolino and F. Simoni, Phys. Rev. E **47**, 3741 (1993).

[20] V. Carbone, G. Cipparrone, C. Versace, C. Umeton and R. Bartolino, Mol. Cryst. Liq. Cryst. Sci. Technol., Sect. A **251**, 167 (1994); V. Carbone, G. Cipparrone, C. Versace, C. Umeton and R. Bartolino, Phys. Rev. E **54**, 6948 (1996); C. Versace, V. Carbone, G. Cipparrone, C. Umeton and R. Bartolino, Mol. Cryst. Liq. Cryst. Sci. Technol., Sect. A**290**, 267 (1996).

[21] E. Santamato, P. Maddalena, L. Marrucci and B. Piccirillo, Liq. Cryst. **25**, 357 (1998); E. Santamato, G. Abbate, P. Maddalena, L. Marrucci, D. Paparo and B. Piccirillo, Mol. Cryst. Liq. Cryst. **328**, 479 (1999).

[22] N. V. Tabiryan, A. L. Tabiryan-Murazyan, V. Carbone, G. Cipparrone, C. Umeton and C. Versace, Optics Commun. **154**, 70 (1998).

[23] G. Demeter and L. Kramer, Phys. Rev. Lett. **83**, 4744 (1999); G. Demeter, Phys. Rev. E **61**, 6678 (2000).

[24] A. Arneodo, P. Coullet and C. Tresser, Phys. Lett. **81A**, 197 (1981); Y. Kuramoto and S. Koga, Phys. Lett. **92A**, 1 (1982).

[25] D. V. Lyubimov and M. A. Zaks, Physica D **9**, 52 (1983).

[26] G. Russo, V. Carbone and G. Cipparrone, Phys. Rev. E **62** 5036 (2000); V. Carbone, G. Cipparrone and G. Russo, Phys. Rev. E **63** 051701 (2001).

[27] G. Demeter and L. Kramer, Phys. Rev. E **64**, 020701 (2001); G. Demeter and L. Kramer: Mol. Cryst. Liq. Cryst. **375**, 745 (2002).

[28] E. Santamato, B. Daino, M. Romagnoli, M. Settembre, and Y.R. Shen, Phys. Rev. Lett. **57**, 2423 (1986).

[29] E. Santamato, M. Romagnoli, M. Settembre, B. Daino, and Y.R. Shen, Phys. Rev. Lett. **61**, 113 (1988).

[30] L. Marrucci, G. Abbate, S. Ferraiuolo, P. Maddalena, and E.Santamato, Phys. Rev. A **46**, 4859 (1992).

[31] R. A. Beth, Phys. Rev. **50**, 115 (1936).

[32] J. D. Jackson, *Classical electrodynamics* (Wiley, New York, 1962).

[33] L. Allen, M. W. Beijersbergen, R. J. C. Spreeuw, and J. P. Woerdmann, Phys. Rev. A **45**, 8185 (1992).

[34] A. S. Zolot'ko, and A. P. Sukhorukov, Sov. Phys. JETP Lett., **52**, 62 (1990).

[35] S. D. Durbin, S. M. Arakelian, and Y. R. Shen, Opt. Lett. **6**, 411 (1981).

[36] E. Brasselet and T. Galstian, Opt. Commun. **186**, 291 (2000).

[37] E. Brasselet, B. Doyon, T.V. Galstian and L. J. Dube, Phys. Lett. A **299**, 212 (2002).

[38] E. Brasselet, B. Doyon, T.V. Galstian and L. J. Dube, Phys. Rev. E **67**, 031706 (2003).

[39] D. O. Krimer, G. Demeter, and L. Kramer, Mol. Cryst. Liq. Cryst. **421**, 117 (2004).

[40] E. Brasselet, T.V. Galstian, L. J. Dube, D. O. Krimer and L. Kramer, J. Opt. Soc. Am. B, **22**, 1671 (2005).

[41] H. L. Ong, Phys. Rev. A **28**, 2393 (1983).

[42] P. Glendinning, *Stability, instability and chaos* (Cambridge University press, Cambridge, 1996).

[43] D. O. Krimer, PhD Thesis (2004).

[44] E. Brasselet, Phys. Lett. A **323**, 234 (2004).

[45] Istvan Janossy, J. Nonlin. Opt. Phys. Mat. **8**, 361 (1999).

[46] L. Marrucci, D. Paparo, P. Maddalena, E. Massera, E. Prudnikova, and E. Santamato, J. Chem. Phys **107**, 9783 (1997).

[47] B. Y. Zel'dovich and N. Tabiryan, Sov. Phys. JETP **55**, 656 (1982).

[48] E. Santamato, G. Abbate, P. Maddalena, L. Marrucci and Y. R. Shen, Phys. Rev. Lett. **64**, 1377 (1990).

[49] A. Vella, B. Piccirillo, and E. Santamato, Phys. Rev. E **65**, 031706 (2002).

[50] D. O. Krimer, L. Kramer, E. Brasselet, T.V. Galstian and L. J. Dube, J. Opt. Soc. Am. B, **22**, 1681 (2005).

[51] L. Csillag, J. Janossy, V. F. Kitaeva, N. Kroo and N. N. Sobolev, Mol. Cryst. Liq. Cryst. **84**, 125 (1982); E. Santamato and Y. R. Shen, Opt. lett. **9**, 564 (1984).

[52] I. C. Khoo, T. H. Liu and P. Y. Yan, J. Opt. Soc. Am. B **4**, 115 (1987).

[53] A. Vella, A. Setaro, B. Piccirillo, and E. Santamato, Phys. Rev. E **67**, 051704 (2003).

[54] F. Lonberg and R. B. Meyer, Phys. Rev. Lett. **55**, 718 (1985).

[55] D. W. Allender, R. M. Hornreich and D. L. Johnson, Phys. Rev. Lett. **59**, 2654 (1987).

[56] M. Argentina, P. Coullet, E. Risler: Phys. Rev. Lett. **86**, 807 (2001).

[57] S. Popp, O. Stiller, I. Aranson and L. Kramer, Physica D **84**, 398 (1995).

[58] Y. Kuramoto: *Chemical Oscillations, Waves and Turbulence*, Springer 1984.

[59] G. Russo, G. Cipparrone and V. Carbone, Europhys. Lett. **63** 180 (2003).

[60] D. O. Krimer, and E. Brasselet, to be published.

[61] E. Brasselet, D. O. Krimer, and L. Kramer, Europ. Phys. J. E **17** (2005).